*energies*

MDPI

*Review*

# Voltage Stability Assessment in Modern Power Systems: A Structured Review of Methods and Indices

**Annalisa Liccardo [1,*], Davide Lauria [2], Francesco Bonavolontà [1], Guido Coletta [3], Giorgio Maria Giannuzzi [3], Salvatore Tessitore [3] and Cosimo Pisani [3]**

[1] Department of Electrical Engineering and Information Technology, University of Naples Federico II, 80125 Naples, Italy; francesco.bonavolonta@unina.it
[2] Department of Industrial Engineering, University of Naples Federico II, 80125 Naples, Italy; davide.lauria@unina.it
[3] Terna S.p.A., 00156 Rome, Italy; guido.coletta@terna.it (G.C.); giorgio.giannuzzi@terna.it (G.M.G.); salvatore.tessitore@terna.it (S.T.); cosimo.pisani@terna.it (C.P.)
* Correspondence: aliccard@unina.it

**Abstract**

The increasing penetration of inverter-based resources and the growing complexity of modern power systems have made voltage stability assessment a critical aspect of transmission network operation. This paper presents a review of the main methods and indices adopted for voltage stability assessment, with emphasis on their applicability to real-time monitoring and inverter-dominated grids. The review covers both long-term and short-term voltage stability approaches, including L-index methods, Jacobian- and singular-value-based techniques, Lyapunov-exponent-based methods, trajectory-based indices, and recent artificial intelligence applications. For each method, the main advantages, limitations, computational requirements, and suitability for PMU-based monitoring are discussed. The analysis shows that no single indicator can fully describe all voltage instability phenomena. Instead, combining complementary static and dynamic indices provides a more complete basis for wide-area monitoring and real-time operational support in future power systems. Moreover, the main open challenges related to threshold definition, robustness under evolving grid conditions, and the integration of data-driven techniques into operational stability assessment schemes are discussed.

**Keywords:** voltage stability assessment; power system stability; inverter-based resources; PMU monitoring; voltage stability indices; transmission networks

Check for updates

Academic Editor: Jianyu Zhou

Received: 13 July 2026
Revised: 11 August 2026
Accepted: 24 August 2026
Published: 27 August 2026

**Copyright:** © 2026 by the authors. Licensee MDPI, Basel, Switzerland. This article is an open access article distributed under the terms and conditions of the Creative Commons Attribution (CC BY) license.

## 1. Introduction

Voltage stability has become one of the most critical challenges in the operation and planning of modern electric power systems. The progressive transition from conventional synchronous generation toward converter-interfaced renewable energy sources, together with the increasing complexity of transmission networks and the continuous growth of electricity demand, has significantly altered the dynamic behavior of power systems. In this evolving scenario, maintaining acceptable voltage profiles under both normal operating conditions and disturbances is becoming increasingly difficult, particularly in weak or heavily stressed networks.

Traditionally, voltage instability phenomena were mainly associated with insufficient reactive power support, long transmission corridors, heavily loaded systems, and the progressive degradation of voltage magnitudes under increasing load demand. However,

the widespread penetration of inverter-based resources (IBRs), such as photovoltaic systems, wind power plants, battery energy storage systems, and HVDC converters, has introduced new operational challenges and dynamic interactions that cannot always be adequately captured using conventional stability assessment approaches [1,2]. Unlike synchronous machines, inverter-based generators are characterized by faster dynamics, limited overload capability, and control-dependent behavior, which strongly influence both short-term and long-term voltage stability mechanisms.

Voltage instability may develop over different time scales and under different physical mechanisms. Long-term voltage instability is generally associated with slow dynamics involving tap changers, reactive power limitations, load recovery mechanisms, and voltage control actions. Conversely, short-term voltage instability is characterized by fast transient phenomena involving induction motors, converter-interfaced generation systems, HVDC links, and fast-reacting loads [3,4]. In modern power systems, these mechanisms are often interconnected, making the evaluation of voltage stability increasingly challenging.

To address these issues, a large variety of voltage stability assessment (VSA) methods and voltage stability indices (VSIs) have been proposed in the literature in recent decades. Classical approaches include Jacobian-based methods, sensitivity analysis, modal analysis, continuation power flow techniques, and loadability indices such as the well-known L-index [5,6]. More recently, measurement-based and model-free approaches relying on synchronized phasor measurements obtained from Phasor Measurement Units (PMUs) have attracted considerable attention due to their suitability for real-time monitoring applications [7,8]. In parallel, data-driven and artificial intelligence techniques have emerged as promising tools for stability prediction and online security assessment [9,10].

Despite the large number of proposed methodologies, no single index or assessment technique is capable of fully characterizing all voltage instability mechanisms in modern power systems. Many approaches exhibit limitations related to computational complexity, sensitivity to measurement noise, dependence on accurate system models, or limited applicability under evolving operating conditions and high penetration of renewable energy sources. Furthermore, the increasing deployment of PMUs and wide-area monitoring systems is shifting the focus from offline security studies toward online and predictive stability assessment schemes.

In this context, this paper presents a structured review of the main methods and indices currently adopted for voltage stability assessment in modern power systems. The review covers both long-term and short-term voltage stability approaches, including model-based, measurement-based, and data-driven techniques. Particular attention is devoted to the applicability of the reviewed methods in modern transmission networks characterized by high penetration of inverter-based resources and the availability of synchronized measurements. The main theoretical principles, advantages, limitations, computational requirements, and practical implementation aspects of each approach are critically discussed.

The remainder of this paper is organized as follows. Section 2 introduces the fundamental concepts of voltage stability and discusses the impact of inverter-based resources. Section 3 presents the classification of voltage stability assessment methodologies. Sections 4 and 5 review the principal long-term and short-term voltage stability assessment methods, respectively. Section 6 provides a comparative synthesis of the reviewed techniques together with practical considerations for their implementation in modern monitoring systems. Finally, Section 7 summarizes the main conclusions and discusses future research directions.

## 2. Voltage Stability in Modern Power Systems

This section establishes the physical background required for the assessment methods reviewed in the remainder of the paper. First, the principal long-term and short-term voltage stability mechanisms are summarized. The discussion then focuses on how inverter-based resources modify these mechanisms through their control-dependent behavior, current limitations, and interaction with network strength.

### 2.1. Fundamentals of Voltage Stability

Voltage stability refers to the ability of a power system to maintain acceptable voltage magnitudes at all buses under normal operating conditions and after being subjected to disturbances [6,11]. Voltage instability generally manifests itself through a progressive and uncontrollable reduction of voltage magnitudes, potentially leading to voltage collapse and widespread service interruptions. The phenomenon is strongly related to the capability of the generation and transmission system to provide the reactive power required by loads and network components.

Traditionally, voltage stability problems have been associated with heavily loaded transmission corridors, insufficient reactive power support, long-distance power transfers, and unfavorable network configurations. Under stressed operating conditions, incremental increases in active and reactive power demand may cause excessive voltage drops, leading the system operating point toward instability regions. In these situations, the Jacobian matrix associated with the power-flow equations progressively becomes ill-conditioned and eventually singular at the voltage-collapse point [6].

Voltage stability assessment must be distinguished from conventional static security analysis. While static security mainly focuses on identifying thermal limit violations and unacceptable voltage magnitudes through steady-state power-flow calculations, voltage stability analysis additionally considers the dynamic evolution of the system following disturbances and the ability of the network to recover acceptable operating conditions [12]. In practice, disturbances may trigger cascading events involving protection systems, generator reactive power limitations, load dynamics, and transmission line outages, potentially resulting in severe voltage degradation or system collapse.

Voltage stability phenomena are commonly classified into long-term and short-term categories according to the dominant dynamics involved and the characteristic time scale of the instability process [2,3]. As illustrated in Figure 1, long-term voltage stability is generally associated with slow dynamics involving on-load tap changers, generator excitation systems, reactive power limitations, thermostatically controlled loads, and voltage control actions. These phenomena typically evolve over time intervals ranging from several seconds to minutes and are often characterized by progressive voltage decay caused by the inability of the system to restore reactive power balance.

Conversely, short-term voltage stability is dominated by fast dynamic phenomena involving induction motors, power-electronic converters, HVDC links, electronically controlled loads, and inverter-based generation systems. The characteristic time scale ranges from fractions of a second to a few seconds following a disturbance [13]. One of the most common mechanisms associated with short-term voltage instability is induction motor stalling. During severe voltage dips, induction motors decelerate while absorbing large amounts of reactive current from the network. If the motor speed falls below a critical threshold, reacceleration may no longer be possible, causing prolonged low-voltage conditions and potentially triggering cascading instability phenomena.

In modern power systems characterized by high penetration of inverter-based resources, the traditional mechanisms of voltage instability are evolving. Converter-interfaced renewable generation can partially decouple mechanical dynamics from grid voltage behav-

ior, reducing the relevance of some classical instability mechanisms while simultaneously introducing new control-related dynamic interactions [4]. Consequently, voltage stability assessment increasingly requires the combined analysis of both static operating conditions and fast dynamic responses.

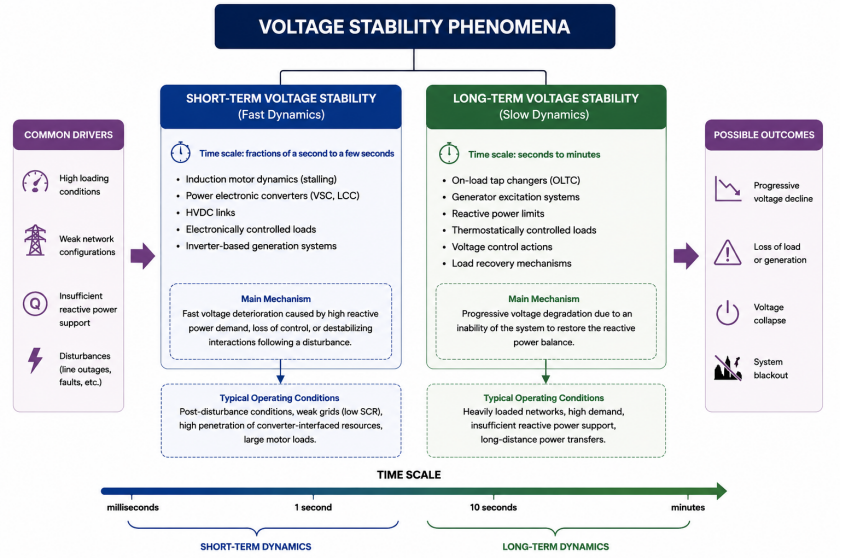



**Figure 1.** Classification of voltage stability phenomena according to dominant dynamics and characteristic time scales.

Typical voltage trajectories associated with stable and unstable operating conditions are illustrated in Figure 2. Following a disturbance, a stable system is characterized by a temporary voltage dip followed by recovery toward an acceptable steady-state condition. Long-term voltage instability generally manifests itself through a slow and progressive voltage degradation, while short-term instability is associated with rapid voltage collapse caused by fast dynamic interactions and insufficient reactive power support.

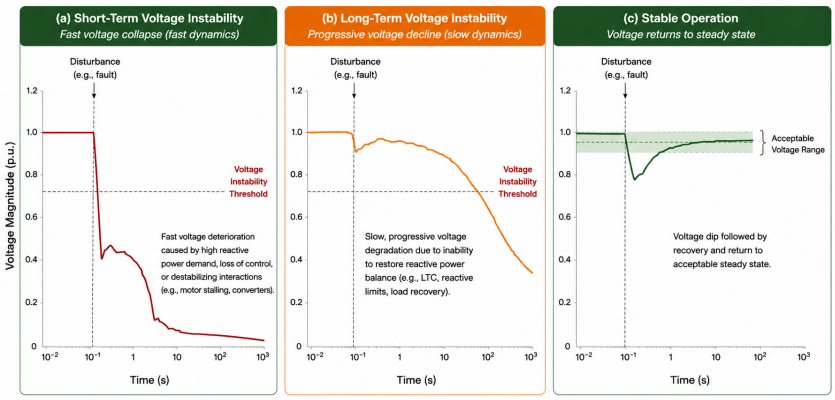



**Figure 2.** Typical voltage trajectories associated with stable operation, long-term voltage instability, and short-term voltage instability following a disturbance.

From an operational perspective, voltage stability is closely connected to the management of reactive power resources throughout the transmission system. Reactive power compensation devices, synchronous condensers, generator excitation systems, static VAR compensators, STATCOMs, and converter-interfaced resources all contribute to maintaining acceptable voltage profiles and preserving adequate stability margins. Accurate voltage stability assessment therefore plays a crucial role in both long-term planning studies and real-time operational decision-making.

### *2.2. The Impact of Inverter-Based Generation Systems on Voltage Stability*

Modern inverter-based generation systems (IBRs) connected to the grid undoubtedly exhibit faster dynamics compared to traditional synchronous generators. The inverter control strategy determines steady-state behavior and naturally dominates transient response following contingencies.

Instability or disconnection of such generation systems can increase power flows, leading to voltage instability, also due to the lack of reactive power support originally provided by these innovative generation systems. Even without disconnection, it should be noted that, under critical conditions, the converter current magnitude may reach its maximum allowable value, so that, behaving as a current source, the overall system may become unstable.

It is therefore crucial that, following a credible contingency, such generation systems remain connected to the grid and effectively contribute to sustaining voltage levels. It is worth highlighting that they must also help mitigate frequency variations, and that instability phenomena may be exacerbated by the intermittent nature of renewable sources.

Critical situations strongly depend on grid strength, also referred to as grid stiffness, widely used to describe the ability of the power system to maintain voltage stability under contingencies. This parameter also significantly influences the synchronization capability of inverters with the grid; when connected to a bus with inadequate short-circuit capacity, loss of stability or oscillations with negative damping may occur.

The parameter SCR (Short Circuit Ratio) is defined to characterize grid strength. If a generic bus is connected to an inverter-based resource, the SCR is defined as:

$$SCR_{\text{bus}} = \frac{MVA_{SC_\text{bus}}}{MW_{\text{rating IBR}}} \tag{1}$$

where $MVA_{SC_\text{bus}}$ is the short-circuit apparent power at the considered bus, while $MW_{\text{rating IBR}}$ represents the rated power of the inverter-based resource connected to the same bus.

This metric is suitable for a single generation system but does not fully account for the presence of nearby generation units. When multiple IBR systems are present, alternative metrics have been proposed, such as the Weighted Short Circuit Ratio (WSCR) [14], defined as:

$$WSCR = \frac{\sum_{i=1}^{n}\left(MVA_{SC_\text{bus},i} \cdot MW_{\text{rating IBR},i}\right)}{\sum_{i=1}^{n}\left(MW_{\text{rating IBR},i}\right)^2} \tag{2}$$

where $MVA_{SC_\text{bus},i}$ is the short-circuit apparent power at the bus connected to the $i$-th inverter-based resource, while $MW_{\text{rating IBR},i}$ is the rated power of the corresponding inverter-based resource.

Several additional metrics have been proposed in the literature to assess system strength in networks with a high penetration of inverter-based resources.

The Composite Short-Circuit Ratio (CSCR) [1] extends the conventional SCR concept by aggregating multiple IBRs electrically close to each other into a composite node. The CSCR is defined as:

$$CSCR = \frac{MVA_{SC\ composite}}{MW_{\text{rating all IBRs}}} \tag{3}$$

where $MVA_{SC\ composite}$ is the short-circuit apparent power at the composite bus, while $MW_{\text{rating all IBRs}}$ represents the total rated power of all inverter-based resources connected within the considered area.

Both the Weighted Short-Circuit Ratio (WSCR) and the Composite Short-Circuit Ratio (CSCR) are based on the assumption that the inverter-based resources are electrically close

to each other. Consequently, they neglect the impedance between converter buses and may not accurately represent systems characterized by strong electrical interactions among geographically distributed IBRs.

To overcome this limitation, the Equivalent Short-Circuit Ratio (EqSCR) was introduced in [15]. EqSCR explicitly accounts for network topology and electrical coupling among multiple inverter-based resources by considering the interaction among converter buses. This allows a more accurate characterization of weak-grid conditions in modern renewable-dominated transmission systems.

When SCR values are inadequate, either synchronous machines, possibly operated as synchronous condensers, must be installed, or inverter operation philosophy must shift toward the grid-forming concept. In this operating mode, the inverter no longer behaves as a current source synchronized to the grid through a phase-locked loop, but emulates the behavior of a synchronous machine by directly regulating voltage magnitude and frequency. Consequently, the converter acts as a voltage source capable of actively supporting system voltage stability.

The type of converter technology also has a significant impact on voltage stability behavior. Line-Commutated Converter (LCC) HVDC systems are characterized by substantial reactive power absorption during disturbances and may therefore aggravate voltage instability phenomena under weak-grid conditions. Conversely, Voltage-Source Converter (VSC) technologies provide enhanced controllability of active and reactive power, allowing improved voltage-support capabilities and more flexible operation [1].

From a voltage-stability-assessment perspective, the influence of inverter-based resources must also be distinguished according to the time scale under consideration. In quasi-steady-state studies, the feasible operating point and the associated power-flow Jacobian depend on the converter reactive-power capability, current limits, active-power set points, plant-level voltage control, and the adopted grid-following or grid-forming control mode. Once a converter reaches its current limit, active and reactive power can no longer be regarded as independently controllable. Consequently, static indices that assume unrestricted reactive-power support may overestimate the actual stability margin.

At the short-term time scale, phase-locked-loop and current-control dynamics, fault-ride-through logic, active- or reactive-current priority, protection settings, and post-fault active-power recovery may dominate the voltage trajectory. Grid-forming control can improve voltage and frequency support in weak networks, but its contribution remains constrained by converter current limits and control settings. Classical model-based indices therefore remain useful for identifying network stress, provided that converter operating modes, controls, and limits are explicitly represented. PMU-based dynamic indices provide complementary information on the actual post-disturbance response and are particularly relevant when fast converter interactions cannot be adequately represented by quasi-steady-state models [1,2,4].

The ongoing transition towards converter-dominated power systems is profoundly changing the mechanisms governing voltage stability. The progressive displacement of synchronous generation by inverter-based resources reduces system strength and modifies the interaction between active power transfer, reactive power support, and voltage regulation. As a result, the classical assumption of a weak coupling between active power flows and voltage magnitudes, which underpins many conventional voltage stability assessment methods, becomes progressively less accurate. Consequently, voltage stability can no longer be regarded solely as a reactive power adequacy problem but should instead be analyzed as the outcome of coupled active and reactive power dynamics, converter control actions, and network strength.

The large-scale blackout that affected the Iberian power system on 28 April 2025 further highlighted the increasing complexity of voltage stability phenomena in converter-rich power systems. According to the final investigation carried out by the ENTSO-E Expert Panel [16], the event resulted from a combination of technical, operational, and control-related factors, with voltage control and reactive power management playing a central role in the cascading sequence of events. Rather than being attributable to renewable generation itself, the disturbance demonstrated how interactions among converter control strategies, network strength, reactive power support, and system operating conditions may significantly influence voltage stability in modern transmission networks. These findings reinforce the need for voltage stability assessment methodologies capable of combining static operating margins with dynamic indicators suitable for real-time monitoring and decision support.

Figure 3 summarizes the main mechanisms through which inverter-based resources influence voltage stability in modern power systems.

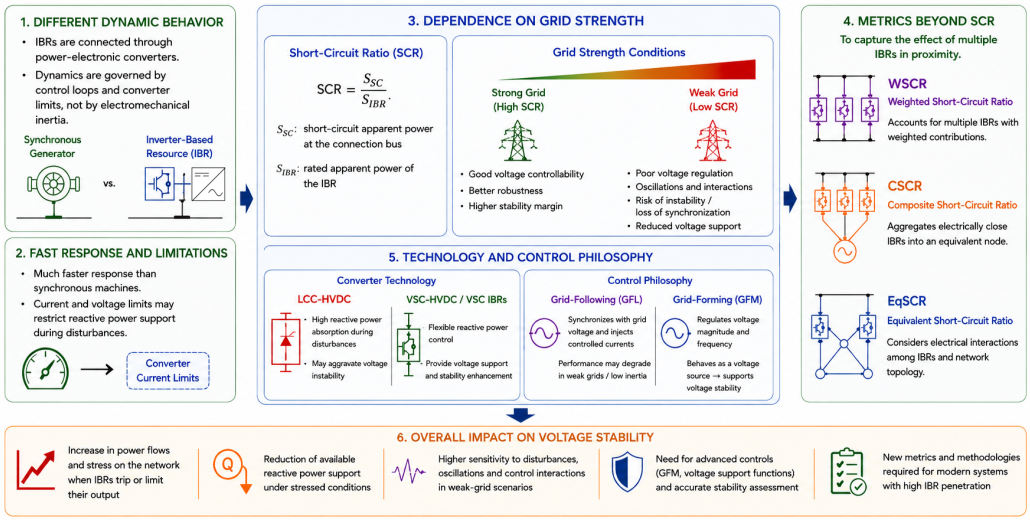



**Figure 3.** Main mechanisms through which inverter-based resources influence voltage stability in modern power systems.

## 3. Approaches for Voltage Stability Assessment

### *3.1. Literature Selection Criteria*

The present study was conducted as a structured narrative review rather than as a formal systematic review performed according to a PRISMA protocol. The literature search was carried out primarily through IEEE Xplore, Scopus, and Web of Science, while Google Scholar was used as a complementary source for citation tracking and the identification of relevant technical reports. The search combined terms such as voltage stability assessment, voltage stability index, voltage collapse, short-term voltage stability, long-term voltage stability, PMU, wide-area monitoring, inverter-based resources, grid-forming converters, Jacobian methods, Lyapunov exponent, and artificial intelligence.

The principal publication window covered the period from 2020 to 2025, while earlier seminal contributions were retained when required to describe the theoretical foundations of the reviewed methods. Eligible sources included peer-reviewed journals and conference papers and authoritative technical reports that proposed, analyzed, or compared voltage-stability assessment methods; addressed long-term or short-term voltage stability; or examined PMU-based monitoring, inverter-dominated systems, or real-time implementation. Duplicate records, non-technical publications, studies concerned exclusively with

voltage control without a stability-assessment component, and works lacking sufficient methodological detail were excluded.

The selected literature was organized according to the characteristic time scale of the instability phenomenon, model dependence, measurement requirements, computational burden, and suitability for online monitoring. Accordingly, the present paper should be interpreted as a structured expert synthesis rather than as an exhaustive systematic mapping of all publications in the field. Official technical reports published in 2026 and available before the final update of the review were additionally considered when directly relevant to recent system events.

### 3.2. Methods for Voltage Stability Assessment

Voltage Stability Assessment (VSA) methodologies can be broadly classified into two main categories: long-term and short-term approaches. Long-term methods are mainly aimed at evaluating the proximity of the system operating point to voltage collapse conditions under quasi-steady-state assumptions, whereas short-term approaches focus on the fast dynamic evolution of voltages following severe disturbances.

From a methodological perspective, long-term voltage stability approaches are generally divided into three main families:

- model-based approaches;
- preventive or hybrid approaches;
- measurement-based approaches.

Model-based techniques rely on detailed knowledge of the network model, including the admittance matrix, generator models, load representations, and power-flow Jacobian matrices. These methods typically include continuation power-flow techniques, sensitivity analysis, modal analysis, singular-value decomposition approaches, and loadability indices. Their main advantage is the strong physical interpretability of the obtained stability margins. However, their practical implementation in real-time operational environments may become challenging because of the need for continuously updated and accurate network models.

Preventive and hybrid approaches combine offline simulations with online monitoring techniques. In these methodologies, large sets of operating conditions and contingencies are analyzed offline in order to identify critical operating regions and derive simplified stability indicators suitable for online deployment. Such approaches provide a compromise between computational efficiency and physical accuracy, allowing operators to estimate stability margins without executing full dynamic simulations in real time.

Measurement-based approaches, on the other hand, exploit synchronized phasor measurements provided by PMUs and Wide Area Monitoring Systems (WAMS). These methods estimate stability margins directly from voltage and current measurements without requiring complete knowledge of the system model. Thévenin-equivalent approaches, impedance-based methods, and data-driven techniques belong to this category. Their main advantage lies in their adaptability under continuously changing operating conditions and in modern grids characterized by high penetration of inverter-based resources.

Figure 4 summarizes the main classification of voltage stability assessment methodologies discussed in this review.

Short-term voltage stability assessment methods are instead primarily focused on the dynamic response of the system immediately following disturbances. These approaches generally rely on high-frequency PMU measurements and are characterized by strict real-time requirements. Because of the need for rapid detection capabilities, short-term methods often avoid detailed parameter estimation and instead process voltage trajectories directly.

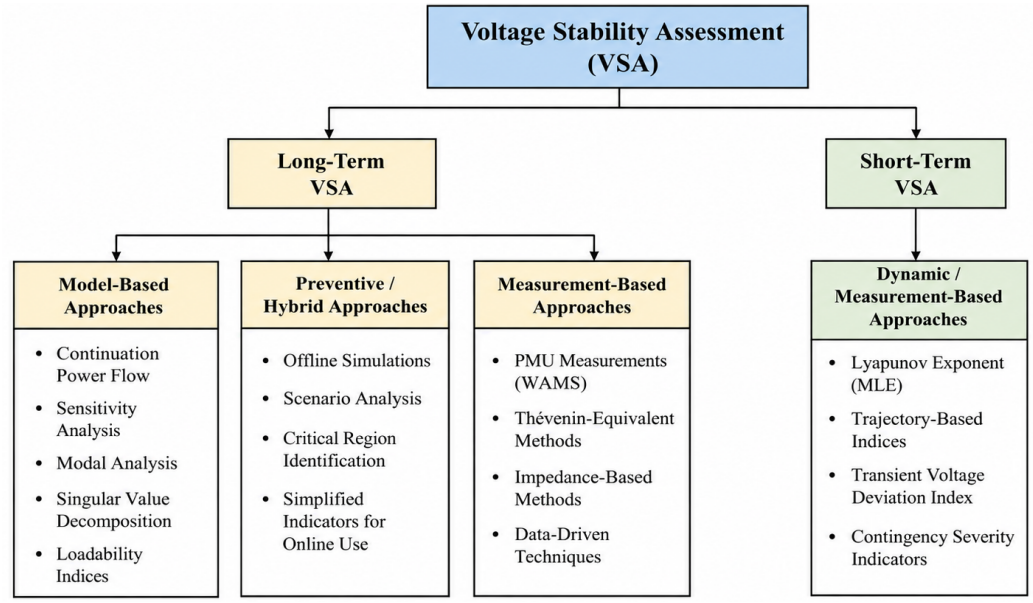



**Figure 4.** Classification of voltage stability assessment methodologies in modern power systems.

Among the most widely investigated short-term indices are Lyapunov-based methods, trajectory-based indices, transient voltage deviation indicators, and contingency severity metrics [3,17]. In particular, Maximum Lyapunov Exponent (MLE)-based approaches are attracting increasing attention because of their model-free nature and their capability to provide early indications of instability directly from measured voltage trajectories.

The different VSA approaches can also be classified according to the amount of information required for their implementation. Some methods require complete network knowledge, including topology and dynamic models, whereas others operate exclusively on local voltage measurements. Similarly, computational requirements may vary significantly among the different techniques. Classical static indices are generally computationally efficient and therefore suitable for online applications, while detailed dynamic simulations and optimization-based methods may become too demanding for real-time deployment.

Another important aspect concerns the applicability of the methods under modern operating conditions characterized by high penetration of renewable energy sources and inverter-based generation. Several traditional approaches were originally developed for synchronous-machine-dominated systems and may therefore require significant adaptations in converter-dominated networks. In particular, the reduction of system inertia, the increasing relevance of converter control dynamics, and the widespread presence of power-electronic interfaces are progressively modifying the mechanisms associated with voltage instability phenomena.

For practical operational deployment, voltage stability assessment techniques should satisfy several important requirements:

- limited computational burden;
- real-time applicability;
- robustness against measurement uncertainty and noise;
- adaptability under varying operating conditions;
- capability to provide sufficiently early warning signals;
- physical interpretability of the obtained stability indicators.

The selection of appropriate indices therefore depends not only on theoretical accuracy but also on operational constraints associated with measurement infrastructures, communication systems, computational platforms, and decision-making procedures adopted by transmission system operators.

### *3.3. Applicability to Converter-Dominated Power Systems*

The increasing penetration of inverter-based resources does not make conventional voltage-stability indices intrinsically invalid, since the algebraic relationships among bus voltages, currents, and power injections remain applicable. However, the operating point represented by these equations and the interpretation of the resulting indices become conditional on the converter control mode, current limits, network strength, and the time scale of interest [14,15]. In systems with high penetration of inverter-based resources, converter controls broaden and couple the frequency ranges traditionally associated with voltage, angle, and frequency stability. Consequently, a quasi-steady-state index should not be interpreted as a complete measure of converter-driven stability [1,2,18,19].

For power-flow-, admittance-, and Jacobian-based methods, the main adaptation concerns the formulation of the operating model rather than the algebraic definition of the index. Inverter-based resources should be represented according to their actual steady-state control objective—for example, constant active and reactive power, voltage/reactive-power control, or grid-forming voltage control—and their reactive-power capability, current saturation, and active/reactive current-priority logic should be taken into account. Published studies show that inverter control modes can materially affect static voltage-stability margins, while current saturation can modify both the feasible power injection and the converter's ability to recover its voltage-control mode after a disturbance [20,21]. Static indices therefore remain useful for screening network stress, but they may overestimate the usable operating margin if converter limits and operating-mode transitions are neglected.

For sensitivity, modal, and singular-value methods, the reduced power-flow Jacobian remains informative when its underlying decoupling assumptions are sufficiently accurate. In weak multi-converter networks, however, phase-locked-loop dynamics, network topology, and converter-to-converter interactions can materially modify synchronization stability margins [22,23]. When active–reactive power coupling is significant, the full power-flow Jacobian should therefore be considered for quasi-steady-state analysis instead of relying exclusively on a strictly decoupled formulation. For small-signal dynamic studies, the linearized differential-algebraic model should include the relevant states of the phase-locked loops, inner current controllers, outer voltage or reactive-power controllers, and grid-forming control loops, according to the frequency range and time scale under investigation.

Measurement-based and trajectory-based indices provide complementary information on the actual post-disturbance response and are less dependent on the explicit representation of proprietary converter controls. Nevertheless, they are not parameter-free: the faster and potentially oscillatory dynamics introduced by inverter-based resources affect the required sampling rate, filtering procedure, numerical differentiation, moving-window length, and decision thresholds. Accordingly, model-based quasi-static indices and PMU-based dynamic indices should be regarded as complementary rather than interchangeable assessment tools [8,19].

## 4. Methods for Long-Term Voltage Stability Assessment

Long-term voltage stability assessment evaluates the proximity of the operating point to voltage-collapse conditions under quasi-steady-state assumptions. The methods reviewed in this section differ in their mathematical formulation, information requirements, computational burden, and suitability for online implementation. Their applicability to converter-dominated systems is interpreted according to the considerations introduced in Sections 2.2 and 3.

### *4.1. Analysis of L-Index*

In the following, reference is made, for the sake of proper and rigorous clarification, to the seminal work [5], which can undoubtedly be regarded as a cornerstone in the field of voltage stability estimation. An index is derived with reference to a simple system and then generalized. The choice to focus on this approach is based on the fact that such an index can be effectively evaluated in the modern context of interconnected power systems, provided that PMUs are suitably distributed throughout the network in order to estimate the system configuration.

#### 4.1.1. Estimation for a Simple Two-Bus System

Consider the system schematically represented in Figure 5.

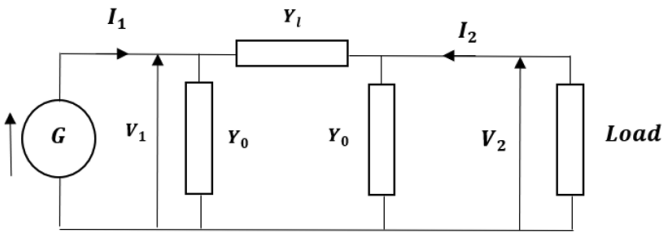



**Figure 5.** Simple system with one generation bus and one load bus.

It is assumed that $\boldsymbol{V}_1$ and $\boldsymbol{V}_2$ are the phasors of the nodal voltages, $\boldsymbol{I}_1$ and $\boldsymbol{I}_2$ are the phasors of the nodal currents, and $\boldsymbol{S}_1$ and $\boldsymbol{S}_2$ denote the corresponding complex powers.

The two-terminal element is fully described by the admittance matrix:

$$\boldsymbol{Y} = \begin{bmatrix} \boldsymbol{Y_{11}} & \boldsymbol{Y_{12}} \\ \boldsymbol{Y_{21}} & \boldsymbol{Y_{22}} \end{bmatrix} \tag{4}$$

It is therefore possible to write the following relation for node 2:

$$\boldsymbol{I_2} = \boldsymbol{Y_{21}V_1} + \boldsymbol{Y_{22}V_2} = \frac{\boldsymbol{S_2}^*}{\boldsymbol{V_2}^*} \tag{5}$$

where $\boldsymbol{S_2}$ is the complex power:

$$\boldsymbol{S_2} = \boldsymbol{V_2 I_2}^* \tag{6}$$

This relation can be rewritten as:

$$V_2^2 + \boldsymbol{V_0 V_2}^* = \frac{\boldsymbol{S_2}^*}{\boldsymbol{Y_{22}}} = \lambda + j\mu \tag{7}$$

where: $\boldsymbol{V_0} = \frac{\boldsymbol{Y_{21}}}{\boldsymbol{Y_{22}}}\boldsymbol{V_1} = -\frac{\boldsymbol{Y_l}}{\boldsymbol{Y_l}+\boldsymbol{Y_0}}\boldsymbol{V_1}$ and $V_2^2$ corresponds to the squared magnitude of $\boldsymbol{V_2}$, computed as $\boldsymbol{V_2 V_2}^*$.

The modulus of $\boldsymbol{V_2}$ is determined from (7) as:

$$V_2 = \sqrt{\frac{V_0^2}{2} + \lambda \pm \sqrt{\frac{V_0^4}{4} + \lambda V_0^2 - \mu^2}} \tag{8}$$

Equation (7) can be expressed in the following form:

$$|\boldsymbol{S_2} - \boldsymbol{Y_{22}}^* V_2^2| = \boldsymbol{V_0 V_2}^* \boldsymbol{Y_{22}} \tag{9}$$

This clearly shows that the operating points, characterized by the pair $P_2, Q_2$ with constant modulus $V_2$, lie on circles in the complex plane $P_2 + jQ_2$, whose center is given by $\boldsymbol{Y_{22}}^* V_2^2$ and the radius is $V_0 V_2 Y_{22}$.

The envelope of these circles provides the stability limit, bearing in mind that system operation is not possible outside this curve. At the envelope, it can be shown that the two roots given by (8) coincide, namely:

$$\sqrt{\frac{V_0^4}{4} + \lambda V_0^2 - \mu^2} = 0 \tag{10}$$

and:

$$V_2 = \sqrt{\frac{V_0^2}{2} + \lambda} \tag{11}$$

From (9), it follows that:

$$\lambda = V_2^2 - \frac{V_0^2}{2} \tag{12}$$

Substituting (12) into (10) allows the calculation of $\mu$:

$$\mu = \sqrt{V_2^2 V_0^2 - \frac{V_0^4}{4}} \tag{13}$$

It is useful to highlight, for reasons that will soon be clear, that:

$$\sqrt{\lambda^2 + \mu^2} = V_2^2 \tag{14}$$

Equation (7) can be expressed as:

$$1 + \frac{\boldsymbol{V_0}}{\boldsymbol{V_2}} = \frac{\boldsymbol{S_2}^*}{\boldsymbol{Y_{22}} V_2^2} = \frac{\lambda + j\mu}{V_2^2} \tag{15}$$

At the instability condition, the modulus leads to:

$$\left|1 + \frac{\boldsymbol{V_0}}{\boldsymbol{V_2}}\right| = \left|\frac{\boldsymbol{S_2}^*}{\boldsymbol{Y_{22}} V_2^2}\right| = \left|\frac{\lambda + j\mu}{V_2^2}\right| = \frac{\sqrt{\lambda^2 + \mu^2}}{V_2^2} = 1 \tag{16}$$

Relation (16) motivates the definition of the indicator $L$:

$$L = \left|1 + \frac{\boldsymbol{V_0}}{\boldsymbol{V_2}}\right| = \left|\frac{\boldsymbol{S_2}^*}{\boldsymbol{Y_{22}} V_2^2}\right| \tag{17}$$

This indicator takes values between 0 and 1.

As highlighted in [5], the fact that index $L$ approximates 1 as an intrinsic measure of stability is linked to the consideration that the load-flow Jacobian becomes singular. For set values of $L$, from (17) it follows that:

$$S_2 = \frac{V_0^2 Y_{22}}{L + \frac{1}{L} - 2\cos(\varphi_{S_2} + \varphi_{Y_{22}})} \tag{18}$$

The curves (18) are ellipses in the $P_2, Q_2$ plane.

#### 4.1.2. Extension of the L Index to a Complex Network

The extension to complex networks obviously requires distinguishing between load buses (PQ type), generation buses (PV type), and the slack bus; therefore, the network model

should be known. Actually, PQ, PV, and slack buses are modeling constructs, recalled here only to frame the theoretical extension of the L-index to multi-bus networks. The practical use of the index requires only the classification into load buses or generation buses.

The interconnected power network is described by the matrix relation:

$$\boldsymbol{I} = \boldsymbol{Y}\boldsymbol{V} \tag{19}$$

This can be partitioned as:

$$\begin{bmatrix} \boldsymbol{I}_L \\ \boldsymbol{I}_G \end{bmatrix} = \begin{bmatrix} \boldsymbol{Y}_{LL} & \boldsymbol{Y}_{LG} \\ \boldsymbol{Y}_{GL} & \boldsymbol{Y}_{GG} \end{bmatrix} \begin{bmatrix} \boldsymbol{V}_L \\ \boldsymbol{V}_G \end{bmatrix} \tag{20}$$

Denoting load buses by the subscript $L$ and generator buses by the subscript $G$, the system (20) can conveniently be put in hybrid form:

$$\begin{bmatrix} \boldsymbol{V}_L \\ \boldsymbol{I}_G \end{bmatrix} = \begin{bmatrix} \boldsymbol{Z}_{LL} & \boldsymbol{F}_{LG} \\ \boldsymbol{K}_{GL} & \boldsymbol{Y}_{GG}^{new} \end{bmatrix} \begin{bmatrix} \boldsymbol{I}_L \\ \boldsymbol{V}_G \end{bmatrix} \tag{21}$$

where the matrices $\boldsymbol{Z}_{LL}$, $\boldsymbol{F}_{LG}$, $\boldsymbol{K}_{GL}$, and $\boldsymbol{Y}_{GG}^{new}$ are:

$$\boldsymbol{Z}_{LL} = \boldsymbol{Y}_{LL}{}^{-1} \qquad \boldsymbol{F}_{LG} = -\boldsymbol{Y}_{LL}{}^{-1}\boldsymbol{Y}_{LG} \qquad \boldsymbol{K}_{GL} = \boldsymbol{Y}_{GL}\boldsymbol{Y}_{LL}{}^{-1} \qquad \boldsymbol{Y}_{GG}^{new} = \boldsymbol{Y}_{GG} - \boldsymbol{Y}_{GL}\boldsymbol{Y}_{LL}{}^{-1}\boldsymbol{Y}_{LG} \tag{22}$$

So it can be written that:

$$\boldsymbol{V}_L = \boldsymbol{Z}_{LL}\boldsymbol{I}_L + \boldsymbol{F}_{LG}\boldsymbol{V}_G \tag{23}$$

It is shown that the matrix $\boldsymbol{F}_{LG}$, obtained from the partitioning of the nodal admittance matrix into sub-matrices, is practically real-valued and the sum of the elements of each row is close to one. If we denote by $n_L$ and $n_G$ the number of load and generator buses respectively, the matrix has dimension $n_L \times n_G$. In particular, in [24] it is demonstrated that if $\det(\boldsymbol{Y}_{LL}) \neq 0$, then the following relation holds:

$$\sum_{i=1}^{n_G} \boldsymbol{F}_{LG,ki} = 1 \tag{24}$$

If $\det(\boldsymbol{Y}_{LL}) = 0$ it can be demonstrated that:

$$\sum_{i=1}^{n_G} \boldsymbol{F}_{LG,ki} \cong 1 \tag{25}$$

This matrix plays a fundamental role in voltage stability analysis, as clearly highlighted below. For each load bus $k \in \boldsymbol{\Omega}_L$, one can write:

$$\boldsymbol{V}_{L,k} = \sum_{j \in \boldsymbol{\Omega}_L} \boldsymbol{Z}_{LL,kj}\boldsymbol{I}_{L,j} + \sum_{i \in \boldsymbol{\Omega}_G} \boldsymbol{F}_{LG,ki}\boldsymbol{V}_{G,ki} \tag{26}$$

having partitioned the set of nodes into two disjoint subsets $\boldsymbol{\Omega}_L$ and $\boldsymbol{\Omega}_G$. Relation (26) can be written as:

$$\boldsymbol{V}_{L,k} + \boldsymbol{V}_{0,k} = \boldsymbol{Z}_{LL,kk}\boldsymbol{I}_{L,k} + \sum_{j \in \boldsymbol{\Omega}_L, j \neq k} \boldsymbol{Z}_{LL,kj}\boldsymbol{I}_{L,j} \tag{27}$$

where

$$\boldsymbol{V}_{0,k} = -\sum_{i \in \Omega_G} \boldsymbol{F}_{LG,ki}\boldsymbol{V}_{G,ki}$$

Multiplying both sides by $\boldsymbol{V}^*_{\boldsymbol{L},k}$ yields:

$$V^2_{L,k} + \boldsymbol{V}_{\boldsymbol{0},k}\boldsymbol{V}^*_{\boldsymbol{L},k} = \boldsymbol{Z}_{\boldsymbol{LL},kk}\boldsymbol{S}^*_{\boldsymbol{L},k} + \boldsymbol{V}^*_{\boldsymbol{L},k}\left(\sum_{j\in\boldsymbol{\Omega}_{\boldsymbol{L}},j\neq k}\boldsymbol{Z}_{\boldsymbol{LL},kj}\boldsymbol{I}_{\boldsymbol{L},j}\right) \tag{28}$$

that is:

$$\left|1 + \frac{\boldsymbol{V}_{\boldsymbol{0},k}\boldsymbol{V}^*_{\boldsymbol{L},k}}{V^2_{L,k}}\right| = \left|\frac{\boldsymbol{Z}_{\boldsymbol{LL},kk}\boldsymbol{S}^*_{\boldsymbol{L},k}}{V^2_{L,k}} + \frac{\boldsymbol{V}^*_{\boldsymbol{L},k}}{V^2_{L,k}}\left(\sum_{j\in\boldsymbol{\Omega}_{\boldsymbol{L}},j\neq k}\boldsymbol{Z}_{\boldsymbol{LL},kj}\boldsymbol{I}_{\boldsymbol{L},j}\right)\right| \tag{29}$$

This can be rewritten in terms of the load powers as:

$$\left|1 + \frac{\boldsymbol{V}_{\boldsymbol{0},k}\boldsymbol{V}^*_{\boldsymbol{L},k}}{V^2_{L,k}}\right| = \left|\frac{\boldsymbol{Z}_{\boldsymbol{LL},kk}\boldsymbol{S}^*_{\boldsymbol{L},k}}{V^2_{L,k}} + \frac{\boldsymbol{V}^*_{\boldsymbol{L},k}}{V^2_{L,k}}\left(\sum_{j\in\boldsymbol{\Omega}_{\boldsymbol{L}},j\neq k}\boldsymbol{Z}_{\boldsymbol{LL},kj}\frac{\boldsymbol{S}^*_{\boldsymbol{L},j}}{\boldsymbol{V}^*_{\boldsymbol{L},j}}\right)\right| \tag{30}$$

Equation (30) directly suggests the extension of the L index, derived for the two-bus system, to a general complex network:

$$L_k = \left|1 + \frac{\boldsymbol{V}_{\boldsymbol{0},k}\boldsymbol{V}^*_{\boldsymbol{L},k}}{V^2_{L,k}}\right| = \left|\frac{\boldsymbol{Z}_{\boldsymbol{LL},kk}\boldsymbol{S}^*_{\boldsymbol{L},k}}{V^2_{L,k}} + \frac{\boldsymbol{V}^*_{\boldsymbol{L},k}}{V^2_{L,k}}\left(\sum_{j\in\boldsymbol{\Omega}_{\boldsymbol{L}},j\neq k}\boldsymbol{Z}_{\boldsymbol{LL},kj}\frac{\boldsymbol{S}^*_{\boldsymbol{L},j}}{\boldsymbol{V}^*_{\boldsymbol{L},j}}\right)\right| \tag{31}$$

where $L_k$ is the local voltage stability indicator of the $k$-th load bus.

It is straightforward to infer that the global voltage stability indicator for the system is:

$$\max_{k\in\boldsymbol{\Omega}_{\boldsymbol{L}}}\{L_k\} = \left(\max\left|1 + \frac{\boldsymbol{V}_{\boldsymbol{0},k}}{\boldsymbol{V}_{\boldsymbol{L},k}}\right|\right)_{k\in\boldsymbol{\Omega}_{\boldsymbol{L}}} = \left(\max\left|1 - \frac{\sum_{i\in\boldsymbol{\Omega}_{\boldsymbol{G}}}\boldsymbol{F}_{\boldsymbol{LG},ki}\boldsymbol{V}_{\boldsymbol{G},ki}}{\boldsymbol{V}_{\boldsymbol{L},k}}\right|\right)_{k\in\boldsymbol{\Omega}_{\boldsymbol{L}}} \tag{32}$$

The evaluation of this index is straightforward and fast, as it does not require computing eigenvalues and eigenvectors of the load-flow Jacobian. However, knowledge of the system nodal admittance matrix is necessary, which can, in any case, be estimated using information provided by suitably distributed PMUs. In this case, however, PMU current measurements—or alternatively active and reactive power measurements enabling current estimation—must be available.

### *4.2. Sensitivity Matrix and Modal Analysis*

As is well known, the linearized model of power flows [25] is expressed as:

$$\begin{bmatrix}\boldsymbol{\Delta P}\\ \boldsymbol{\Delta Q}\end{bmatrix} = [\boldsymbol{J}]\begin{bmatrix}\boldsymbol{\Delta V}\\ \boldsymbol{\Delta\theta}\end{bmatrix} = \begin{bmatrix}\boldsymbol{J_{PV}} & \boldsymbol{J_{P\theta}}\\ \boldsymbol{J_{QV}} & \boldsymbol{J_{Q\theta}}\end{bmatrix}\begin{bmatrix}\boldsymbol{\Delta V}\\ \boldsymbol{\Delta\theta}\end{bmatrix} \tag{33}$$

where $\boldsymbol{\Delta P}$ and $\boldsymbol{\Delta Q}$ are the nodal active and reactive power variations around the operating point, and $\boldsymbol{\Delta V}$ and $\boldsymbol{\Delta\theta}$ the vectors of variations in magnitudes and phases of the nodal voltages. From (33) it is easy to demonstrate that:

$$\begin{bmatrix}\boldsymbol{\Delta Q}\\ \boldsymbol{\Delta\theta}\end{bmatrix} = \begin{bmatrix}\boldsymbol{J_{QV}} - \boldsymbol{J_{Q\theta}}\boldsymbol{J_{P\theta}}^{-1}\boldsymbol{J_{PV}} & \boldsymbol{J_{Q\theta}}\boldsymbol{J_{P\theta}}^{-1}\\ -\boldsymbol{J_{P\theta}}^{-1}\boldsymbol{J_{PV}} & \boldsymbol{J_{P\theta}}^{-1}\end{bmatrix}\begin{bmatrix}\boldsymbol{\Delta V}\\ \boldsymbol{\Delta P}\end{bmatrix} \tag{34}$$

If $\boldsymbol{\Delta P} = 0$ holds, the following variation model applies:

$$\boldsymbol{\Delta Q} = \boldsymbol{J_{Q,red}}\boldsymbol{\Delta V} \tag{35}$$

where:

$$\boldsymbol{J_{Q,red}} = \boldsymbol{J_{QV}} - \boldsymbol{J_{Q\theta}}\boldsymbol{J_{P\theta}}^{-1}\boldsymbol{J_{PV}}$$

Thus, the sensitivity matrix

$$S_Q = J_{Q,red}{}^{-1} = \left(J_{QV} - J_{Q\theta}J_{P\theta}{}^{-1}J_{PV}\right)^{-1}$$

can be defined.

The matrix $S_Q$, therefore, expresses the system's response, in terms of changes in nodal voltages, to variations in the reactive power demanded by the network.

An alternative way to evaluate sensitivity, which is more efficient because it allows the analysis to focus on the most critical nodes, is based on the modal analysis of the reduced Jacobian [6]. On the other hand, the sensitivity matrix is closely related to the reduced Jacobian.

In particular, sensitivity can also be assessed by analyzing the eigenvalues of the reduced Jacobian. Let $X$ and $Y$ be the matrices of right and left eigenvectors of $J_{Q,red}$, and $\Lambda$ the matrix of eigenvalues. It follows that $Y = X^{-1}$.

Equation (35) can be expressed as:

$$\Delta Q = J_{Q,red}\Delta V = X\Lambda X^{-1}\Delta V \tag{36}$$

That is:

$$X^{-1}\Delta Q = \Lambda X^{-1}\Delta V \tag{37}$$

Defining vectors

$$\Delta Q_m = X^{-1}\Delta Q = Y\Delta Q$$

and

$$\Delta V_m = X^{-1}\Delta V = Y\Delta V$$

one obtains:

$$\Delta Q_m = \Lambda\Delta V_m \tag{38}$$

This is equivalent, if $n$ is the number of buses, to $n$ decoupled systems:

$$\frac{\Delta V_{m,i}}{\Delta Q_{m,i}} = \frac{1}{\lambda_i} \tag{39}$$

The instability condition emerges when $\lambda_i \to 0$. The eigenvalues $\lambda_i$ thus quantify how incremental changes in reactive power injections affect nodal voltage magnitudes, and therefore provide a direct indication of the system's proximity to voltage instability. In stable operating conditions, small variations in nodal voltages correspond to changes in reactive power. The eigenvalues of the reduced Jacobian are therefore stable and relatively large in magnitude.

As the operating point approaches the voltage-collapse region, however, the Jacobian of the power-flow equations becomes ill-conditioned and its smallest eigenvalue tends toward zero. This results in a sharp increase in the magnitude of the sensitivity coefficients, which effectively diverge as the system approaches the bifurcation point.

The singular value decomposition of the reduced Jacobian is generally more effective than a conventional eigenvalue analysis for assessing network sensitivity and stability. While eigenvalues describe the intrinsic dynamic modes of the system, they do not quantify how close the reduced Jacobian is to singularity nor how strongly small perturbations are amplified. The singular values, and in particular the smallest one, provide a direct measure of the conditioning of the reduced Jacobian and therefore of the system's sensitivity to variations in reactive power or operating conditions. Moreover, the SVD separates the dominant input–output directions, allowing the identification of the most critical nodes

and disturbance patterns, something that the eigenvalue structure alone cannot reveal. For these reasons, the SVD offers a more robust and informative framework for evaluating voltage stability margins and the overall fragility of the network [6].

Therefore, the minimum singular value is typically preferred as a stability-oriented sensitivity index:

$$\sigma_{\min} = \min_{i=1,\ldots,n} \sigma_i$$

where

$$\boldsymbol{\Sigma} = \mathrm{diag}(\sigma_1, \sigma_2, \ldots, \sigma_n)$$

and

$$\boldsymbol{J_{Q,red}} = \boldsymbol{U\Sigma W}^T$$

The smallest singular value, in particular, reflects the system's minimum stability margin and its structural fragility.

### *4.3. Voltage Stability and Solvability of the Reactive Power Sharing Problem*

Suppose that the nodal susceptance matrix is partitioned, distinguishing PV buses and PQ buses, as follows:

$$\boldsymbol{B} = \begin{bmatrix} \boldsymbol{B_{LL}} & \boldsymbol{B_{LG}} \\ \boldsymbol{B_{GL}} & \boldsymbol{B_{GG}} \end{bmatrix} \tag{40}$$

Disregarding shunt susceptances and assuming no phase-shifters, matrix $\boldsymbol{B_{LL}}$ is a Metzler matrix with eigenvalues having negative real parts. The graph associated with matrix $\boldsymbol{B_{LL}}$ is connected. Since, under normal operation, nodal voltage phase angles are small, the reactive power sharing mechanism can, under these assumptions, be described by the following decoupled model:

$$\boldsymbol{Q} = -\mathbf{diag}(\boldsymbol{V})\boldsymbol{BV} \tag{41}$$

where $\boldsymbol{V} = [\boldsymbol{V_L}^T, \boldsymbol{V_G}^T]$ and $\boldsymbol{Q} = [\boldsymbol{Q_L}^T, \boldsymbol{Q_G}^T]$. In this formulation, $\boldsymbol{V}$ denotes the vector containing the magnitudes of the nodal voltages. It is thus possible to write:

$$\boldsymbol{Q_L} = -\mathbf{diag}(\boldsymbol{V_L})(\boldsymbol{B_{LL}V_L} + \boldsymbol{B_{LG}V_G}) \tag{42}$$

Voltages in the absence of reactive power demand can be defined as follows:

$$\boldsymbol{V_L}^* = -\boldsymbol{B_{LL}}^{-1}\boldsymbol{B_{LG}V_G} \tag{43}$$

The following relationship holds:

$$\boldsymbol{Q_L} = -\mathbf{diag}(\boldsymbol{V_L})\boldsymbol{B_{LL}}(\boldsymbol{V_L} - \boldsymbol{V_L}^*) \tag{44}$$

The critical load matrix $\boldsymbol{Q_{crit}}$ can be associated with vector $\boldsymbol{V_L}^*$:

$$\boldsymbol{Q_{crit}} = -\frac{1}{4}\mathbf{diag}(\boldsymbol{V_L}^*)\boldsymbol{B_{LL}}\mathbf{diag}(\boldsymbol{V_L}^*) \tag{45}$$

It is shown [11,26,27] that $\left\|\boldsymbol{Q_{crit}}^{-1}\boldsymbol{Q_L}\right\|_\infty$ measures the distance from voltage collapse; more specifically, if $\left\|\boldsymbol{Q_{crit}}^{-1}\boldsymbol{Q_L}\right\|_\infty < 1$, problem (45) admits one and only one solution. It is straightforward, in the context of voltage stability, to refer to the normalized voltage vector:

$$\boldsymbol{v} = \mathbf{diag}(\boldsymbol{V_L}^*)^{-1}\boldsymbol{V_L} \tag{46}$$

Therefore, Equation (44) can be written as:

$$\boldsymbol{Q_L} = -4\mathbf{diag}(\boldsymbol{v})\boldsymbol{Q_{crit}}(\boldsymbol{v} - \mathbf{1}) \tag{47}$$

which is particularly meaningful, since it expresses the mechanism of reactive power distribution in terms of the matrix $\boldsymbol{Q_{crit}}$.

In ref. [27], the network stress measure is conveniently defined as:

$$\boldsymbol{J_{stress}}(\boldsymbol{v}) = \|\boldsymbol{v} - \mathbf{1}\|_\infty \tag{48}$$

This formulation is naturally suited to frame the problem of stress minimization. If one wishes to limit voltage magnitude deviations with respect to a reference value $V_{ref}$ within a tolerance band $\delta$, by acting on controllable reactive power resources $\boldsymbol{Q_C}$, with size $n_L \times 1$ the following constrained optimization model can be written:

$$\begin{aligned} \min_{Q_c} \quad & \{\boldsymbol{J_{stress}}(\boldsymbol{v})\} \\ \text{s.t.} \quad & \boldsymbol{Q_L} + \boldsymbol{Q_c} = -4\mathbf{diag}(\boldsymbol{v})\boldsymbol{Q_{crit}}(\boldsymbol{v} - \mathbf{1}) \\ & \frac{\left\|\mathbf{diag}(\boldsymbol{V_L}^*)\boldsymbol{v} - V_{ref}\mathbf{1}\right\|_\infty}{V_{ref}} \leq \delta \\ & -\boldsymbol{Q_{c,\min}} \leq \boldsymbol{Q_c} \leq \boldsymbol{Q_{c,\max}} \end{aligned} \tag{49}$$

Problem (49) is non-convex but can be solved without major difficulties. In [27], a linearization procedure is proposed to transform it into a convex optimization problem. However, computational complexity is not discussed; the authors, in fact, focus their attention on the planning-oriented validation and do not take into account real-time implementation.

### *4.4. Determination of the Minimum Distance from the Instability Condition*

It is essential, starting from a given operating condition, to estimate the minimum distance from the instability condition in terms of the active and reactive load power. The following section outlines, in a schematic way, the methodology described in [25].

As already discussed, at the point of voltage instability, the Jacobian matrix of the system of equations that describes the power flow distribution mechanism becomes singular. It is useful to express this model in the following form:

$$\boldsymbol{f}(\boldsymbol{x}, \boldsymbol{\rho}) = \begin{bmatrix} \boldsymbol{g_1}(\boldsymbol{x}) \\ \boldsymbol{g_2}(\boldsymbol{x}) \end{bmatrix} - \begin{bmatrix} \boldsymbol{P} \\ \boldsymbol{Q} \end{bmatrix} = \begin{bmatrix} \boldsymbol{g_1}(\boldsymbol{V}, \boldsymbol{\theta}) \\ \boldsymbol{g_2}(\boldsymbol{V}, \boldsymbol{\theta}) \end{bmatrix} - \begin{bmatrix} \boldsymbol{P} \\ \boldsymbol{Q} \end{bmatrix} = \begin{bmatrix} \boldsymbol{g_1}(\boldsymbol{V}, \boldsymbol{\theta}) \\ \boldsymbol{g_2}(\boldsymbol{V}, \boldsymbol{\theta}) \end{bmatrix} - \boldsymbol{\rho} = 0 \tag{50}$$

where $[\boldsymbol{x}] = [\boldsymbol{V}, \boldsymbol{\theta}]^T$ is the state variable vector, having set

$$\boldsymbol{\rho} = \begin{bmatrix} \boldsymbol{P} \\ \boldsymbol{Q} \end{bmatrix}.$$

If we denote by $\boldsymbol{J_x}$ and $\boldsymbol{J_\rho}$ the Jacobian matrices of the vector function $\boldsymbol{f}$ with respect to $\boldsymbol{x}$ and $\boldsymbol{\rho}$, respectively, the system reaches the instability condition when the parameter $\boldsymbol{\rho}$ and the corresponding state variable vector $\boldsymbol{x}$ are such that the Jacobian $\boldsymbol{J_x}(\boldsymbol{x}, \boldsymbol{\rho})$ becomes singular. It is therefore possible to define a characteristic hypersurface $\boldsymbol{S}$ such that, for every point on it, $\boldsymbol{J_x}(\boldsymbol{x}, \boldsymbol{\rho})$ is singular.

Suppose we have a given operating condition, characterized by $(\boldsymbol{x_0}, \boldsymbol{\rho_0})$. The goal is to determine the load power setting $(\boldsymbol{P}, \boldsymbol{Q})$ that corresponds to the minimum distance between the point $(\boldsymbol{x_0}, \boldsymbol{\rho_0})$ and the hypersurface $S$, which is assumed to be smooth.

This search can be carried out according to the graphical procedure illustrated in Figure 6, where, for the sake of representation, the problem is depicted in the P–Q plane for a single load.

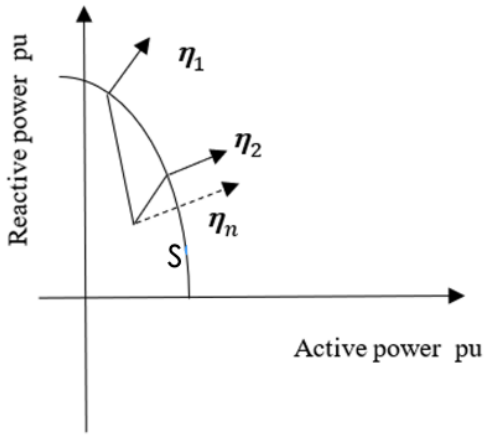



**Figure 6.** Graphical procedure for the determination of the minimum distance from the instability condition.

Given the initial condition $(\boldsymbol{x_0}, \boldsymbol{\rho_0})$, $\boldsymbol{\rho}$ is incremented in an assigned direction so as to reach, at $(\boldsymbol{x_*}, \boldsymbol{\rho_*})$, the singularity condition of the Jacobian $\boldsymbol{J_x}(\boldsymbol{x_*}, \boldsymbol{\rho_*})$. A normal vector to the hypersurface $S$ is given by:

$$\eta_* = \boldsymbol{w_* J_\rho}(\boldsymbol{x_*}, \boldsymbol{\rho_*}) \tag{51}$$

where $\boldsymbol{w_*}$ is the left eigenvector corresponding to the zero eigenvalue of $\boldsymbol{J_x}(\boldsymbol{x_*}, \boldsymbol{\rho_*})$. The determination of the minimum distance is then carried out according to the following iterative procedure:

(a) An initial direction $\boldsymbol{\eta_0}$ with $\|\boldsymbol{\eta_0}\| = 1$ is chosen;
(b) $\boldsymbol{\rho}$ is varied along the direction $\boldsymbol{\eta_i}$ in order to reach the singularity condition of the Jacobian $\boldsymbol{J_x}(\boldsymbol{x_i}, \boldsymbol{\rho_i})$ for $k_i$ such that $\boldsymbol{\rho_i} = \boldsymbol{\rho_0} + k_i \boldsymbol{\eta_i}$;
(c) $\boldsymbol{\eta_{(i+1)}} = \boldsymbol{w_i J_\rho}(\boldsymbol{x_i}, \boldsymbol{\rho_i})$ is set with $\|\boldsymbol{\eta_{(i+1)}}\| = 1$;
(d) Steps a, b, and c are iterated until $\boldsymbol{\eta_i} \rightarrow \boldsymbol{\eta_*}$.

The initial direction $\boldsymbol{\eta_0}$ can be chosen, for example, as the left eigenvector corresponding to the minimum eigenvalue of the Jacobian $\boldsymbol{J_\rho}(\boldsymbol{x_0}, \boldsymbol{\rho_0})$.

It is worth mentioning the continuation power-flow analysis as a tool for voltage stability analysis. The Jacobian matrix of the system of equations describing the distribution of active and reactive power flows becomes singular at the stability limit. This method allows the problem to be reformulated so that it remains well-conditioned for any loading condition [25].

In the case of a two-bus system, for example, it enables the complete determination of the nose curve, i.e., both its upper and lower branches.

### *4.5. Estimation of Voltage Instability by First Order and Second-Order Derivative of Nodal Voltages*

Assuming that the voltage magnitude of the generic $i$-th node is characterized by a single stable or unstable aperiodic mode [28]:

$$V_i(t) = \Gamma_i e^{\gamma t} \tag{52}$$

We have:

$$\begin{aligned} \frac{dV_i(t)}{dt} &= \gamma \Gamma_i e^{\gamma t} \\ \frac{d^2V_i(t)}{dt^2} &= \gamma^2 \Gamma_i e^{\gamma t} \end{aligned} \tag{53}$$

If the system is unstable $(\gamma > 0)$, then: (1) If $\Gamma_i > 0$:

$$\begin{aligned} \frac{dV_i(t)}{dt} &> 0 \\ \frac{d^2V_i(t)}{dt^2} &> 0 \end{aligned} \tag{54}$$

(2) If $\Gamma_i < 0$:

$$\begin{aligned} \frac{dV_i(t)}{dt} &< 0 \\ \frac{d^2V_i(t)}{dt^2} &< 0 \end{aligned} \tag{55}$$

That is, the derivatives have the same sign. As can be seen from Figure 7, in the case of instability, the voltage trajectory moves further and further away from the equilibrium point, either increasing or decreasing according to the value of $\Gamma_i$.

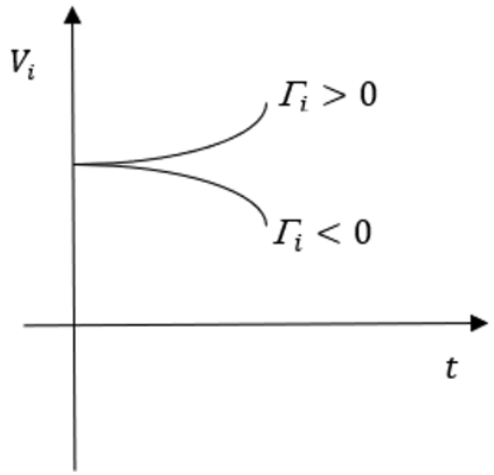



**Figure 7.** Possible voltage trajectories in case of instability.

If the system is stable $(\gamma < 0)$, then (1) if $\Gamma_i > 0$:

$$\begin{aligned} \frac{dV_i(t)}{dt} &< 0 \\ \frac{d^2V_i(t)}{dt^2} &> 0 \end{aligned} \tag{56}$$

(2) If $\Gamma_i < 0$:

$$\begin{aligned} \frac{dV_i(t)}{dt} &> 0 \\ \frac{d^2V_i(t)}{dt^2} &< 0 \end{aligned} \tag{57}$$

The derivatives have opposite signs.

This method, when extended to all nodes of the network, potentially allows the detection of instability conditions based solely on the knowledge of the voltage magnitudes, without requiring knowledge of the full state variables. Moreover, the sign of $\Gamma_i$ provides useful information about the direction of the instability, which can be exploited for diag-

nostic purposes. Another important benefit is its low computational cost, which allows for fast implementation and real-time response.

However, the method also has some limitations. It is valid only for small perturbations around the equilibrium point, which may restrict its applicability in highly nonlinear or large-disturbance scenarios. In addition, appropriate filtering techniques must be applied to the measured signals in order to compute meaningful derivatives and avoid numerical errors. The filter complexity depends on the noise affecting the voltage measurements; a dedicated experimental campaign should be conducted in order to identify the most suitable numerical filter and to estimate the resulting increase in computational complexity.

### *4.6. Estimation of the Network Model Parameters*

Traditional voltage stability analysis relies on knowledge of the network topology. A natural question is whether one can bypass the model and develop a fully data-driven platform. The answer is affirmative, also due to the extensive research efforts devoted to this area.

Regarding Jacobian estimation, as described in [29], one can use a stochastic load model, where voltage magnitudes and phase variations at bus $k$ are described as:

$$\begin{aligned} d\theta_k &= \frac{1}{\tau_{\theta_k}}(P_k - P_k^s) - \frac{1}{\tau_{\theta_k}} P_k^s \sigma_k^P d\xi_k^P \\ dV_k &= \frac{1}{\tau_{V_k}}(Q_k - Q_k^s) - \frac{1}{\tau_{V_k}} Q_k^s \sigma_k^Q d\xi_k^Q \end{aligned} \tag{58}$$

In Equation (58), $\theta_k$ and $V_k$ represent the phase and the magnitude of the voltage at node $k$; $P_k$ and $Q_k$ are the active and reactive power values absorbed at node $k$; $P_k^s$ and $Q_k^s$ are the active and reactive power values under steady-state conditions; $\sigma_k^P$ and $\sigma_k^Q$ are the standard deviations of the two stochastic processes associated with active and reactive power demands; $\tau_{\theta_k}$ and $\tau_{V_k}$ are the time constants associated with the two stochastic processes, related to the "active and reactive power recovery" mechanism; and $d\xi_k^P$ and $d\xi_k^Q$ are two Wiener processes.

These relations can be compactly expressed as a vector Ornstein–Uhlenbeck process:

$$d\boldsymbol{x} = \boldsymbol{A}\boldsymbol{x}dt + \boldsymbol{H}d\xi \tag{59}$$

where:

$$\boldsymbol{x} = [\boldsymbol{\theta}, \boldsymbol{V}]^T;$$

$$\boldsymbol{A} = \begin{matrix} \boldsymbol{T_\theta}^{-1}\frac{\partial \boldsymbol{P}}{\partial \boldsymbol{\theta}} & \boldsymbol{T_\theta}^{-1}\frac{\partial \boldsymbol{P}}{\partial \boldsymbol{V}} \\ \boldsymbol{T_V}^{-1}\frac{\partial \boldsymbol{Q}}{\partial \boldsymbol{\theta}} & \boldsymbol{T_V}^{-1}\frac{\partial \boldsymbol{Q}}{\partial \boldsymbol{V}} \end{matrix} = \begin{matrix} \boldsymbol{T_\theta}^{-1}\boldsymbol{J_{P\theta}} & \boldsymbol{T_\theta}^{-1}\boldsymbol{J_{PV}} \\ \boldsymbol{T_V}^{-1}\boldsymbol{J_{Q\theta}} & \boldsymbol{T_V}^{-1}\boldsymbol{J_{QV}} \end{matrix};$$

$$\boldsymbol{H} = \begin{matrix} \boldsymbol{T_\theta}^{-1}\boldsymbol{P_s}\boldsymbol{\Sigma}^{\boldsymbol{P}} & \boldsymbol{0} \\ \boldsymbol{0} & \boldsymbol{T_V}^{-1}\boldsymbol{Q_s}\boldsymbol{\Sigma}^{\boldsymbol{Q}} \end{matrix};$$

$$\boldsymbol{\xi} = [\boldsymbol{\xi}^{\boldsymbol{P}}, \boldsymbol{\xi}^{\boldsymbol{Q}}]^T.$$

The estimation of matrix $A$ can be effectively carried out based on the covariance and autocorrelation matrices computed over the time window of the phase and voltage magnitude measurements provided by the PMUs [28].

As for estimating the nodal admittance matrix, it can be treated as an inverse problem [30], and under mild assumptions can be formulated as an optimization problem using available voltage and current measurements.

To estimate the network admittance matrix $Y$ from measurement data, the problem can be formulated as a linear inverse problem and solved using a least-squares approach. For an $n$-node network, the synchronous voltage measurements $V(t_m) \in \mathbb{C}^n$ and current injection measurements $I(t_m) \in \mathbb{C}^n$ (e.g., from PMUs) are related by the nodal equation $I = YV$. By collecting $M$ measurement samples, we can state the least-squares problem as:

$$\min_{Y \in \mathbb{C}^{n \times n}} \sum_{m=1}^{M} \| I(t_m) - YV(t_m) \|_2^2 \tag{60}$$

Defining the data matrices:

$$I = [I(t_1)\ I(t_2)\ \cdots\ I(t_M)] \in \mathbb{C}^{n \times M},$$

$$V = [V(t_1)\ V(t_2)\ \cdots\ V(t_M)] \in \mathbb{C}^{n \times M}$$

the problem can be compactly expressed as:

$$\min_{Y} \| I - YV \|_F^2 \tag{61}$$

where the subscript $F$ indicates the Frobenius norm.

If $V$ has full row rank (i.e., $VV^H$ is invertible), the least-squares solution is:

$$Y^\star = IV^H \left( VV^H \right)^{-1} = IV^\dagger \tag{62}$$

## 5. Indeces Tailored to Short-Term Stability

In the following section, the outcomes of the literature review focused specifically on short-term stability indices are presented. These indices are designed to capture instability phenomena characterized by faster and more pronounced dynamics

### *5.1. Short-Term Stability Overview*

Short-term voltage instability refers to a rapid degradation of voltage caused by fast-reacting load components such as induction motors, electronically controlled devices, HVDC interconnections, and inverter-based generation [4]. Another perspective defines it as the inability of the grid to supply the required power to its connected loads [3]. Among the main triggers, the stalling of motors and HVDC links tied to weak AC networks are most often cited. When motors stall, they draw exceptionally high levels of reactive current, heavily stressing both distribution and, at times, transmission systems. This can initiate cascading events and lead to an abrupt voltage collapse with widespread consequences [17,31].

The growing penetration of renewable energy sources (RES) further complicates the short-term voltage instability phenomenon, as their influence can either mitigate or exacerbate instability depending on operating conditions. Following a disturbance, the combined dynamics of induction motors, distributed energy resources (DERs), and their control systems heighten the importance of closely monitoring and predicting potential instabilities. Several of the key drivers of short-term instability have been thoroughly investigated in [13,32]. By nature, short-term voltage instability unfolds within a timescale of a few seconds, which makes real-time analysis and prediction extremely challenging.

In the examined literature, the broader category of short-term instability is divided into four sub-phenomena: short-term voltage instability (STVI), transient rotor angle instability (TRAI), fault-induced delayed voltage recovery (FIDVR), and converter-driven slow interaction instability (CSII). These categories are often interrelated, as they occur on

comparable timescales. Figure 8 illustrates this classification, together with example voltage trajectories for each mechanism, adapted from [3] for illustrative purposes. Although specific system conditions or fault scenarios may lead to different waveforms, the general patterns are representative.

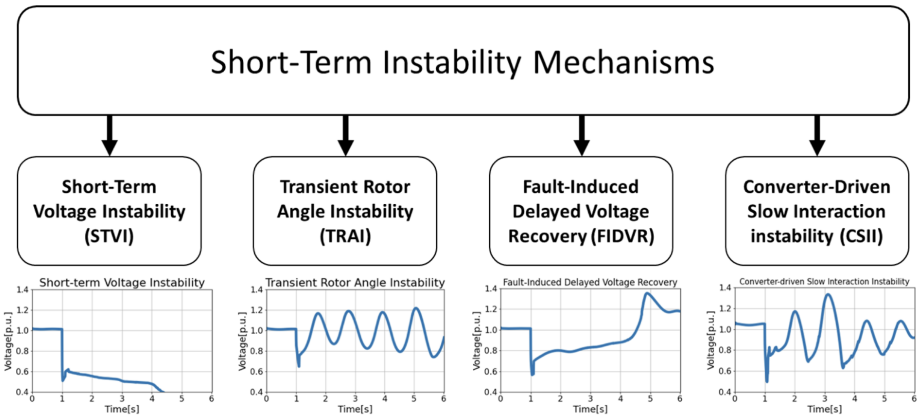



**Figure 8.** Classification of short-term instability phenomena [3].

Among the four, STVI is the most established and widely recognized short-term voltage phenomenon. It is marked by a sharp and irreversible voltage decline following a severe disturbance, where the system fails to restore voltage levels, ultimately leading to collapse. This behavior is illustrated by the STVI trajectory shown in Figure 8.

TRAI, more commonly referred to simply as transient instability, is another classic problem. It describes the loss of synchronism among synchronous generators (or interconnected systems) after a major disturbance [4]. Physically, the instability arises from a breakdown in the torque balance, which accelerates or decelerates the rotor. If the rotor angle exceeds its stability threshold, undamped oscillations emerge, eventually leading to the out-of-step condition. Loss of synchronism may occur immediately after the first oscillation (first-swing instability) or after multiple undamped swings, as illustrated in Figure 8.

FIDVR, in contrast, is a relatively recent focus in both academia and industry. It is characterized by an excessively slow recovery of voltage after a disturbance, often followed by an overshoot. The phenomenon is rooted in transmission–distribution interactions: a sharp transmission voltage dip increases reactive power demand in distribution networks. This effect is frequently associated with air-conditioning compressor motors, although other induction-motor loads may also contribute [3,32]. Stalled motors depress the voltage for tens of seconds until they are disconnected by thermal protections, at which point voltage often spikes. The exact duration of FIDVR events depends on the protection settings of numerous motors across the system. While FIDVR alone is not always an instability, it can trigger cascading effects as multiple elements disconnect under prolonged low-voltage stress. Its typical voltage trajectory is shown in Figure 8.

CSII is included in the four-part classification of short-term instability adopted in [3]. With the rapid growth of RES, these effects are increasingly relevant. CSII arises from slow interactions between IBG control systems and other elements of the power system, including synchronous generators. Although primarily a small-signal stability issue, large disturbances can also excite CSII, producing effects similar to other short-term phenomena. The scope of CSII is broad and can influence both voltage and frequency stability. In this paper, however, it is treated mainly as a voltage-related issue, as inverter control schemes can strongly affect short-term voltage dynamics. Figure 8 presents an illustrative case of CSII, though it is not exhaustive of the many possible converter-driven responses.

Other types of instability, such as slow frequency instability, are not explicitly addressed here. This phenomenon relates more closely to the balance of active power and system inertia than to voltage deviations [4]. Nonetheless, it is possible for the events shown in Figure 8 to eventually evolve into frequency instability. Similarly, short-term resonance stability is excluded from this discussion for analogous reasons.

As indicated, all four instability types occur on a comparable short timescale, making them difficult to distinguish, particularly in real-time applications. Moreover, they are often interconnected, where one event can act as a trigger for another. For example, FIDVR may escalate into large-scale voltage instability or rotor angle instability, while rotor angle instability can precipitate STVI and vice versa. FIDVR has also been shown to create imbalances that can evolve into short-term frequency instability. Such interdependencies are especially concerning in systems with high RES penetration, where severe disturbances can cause widespread disconnections. Given the intertwined nature of these events, modern power systems require comprehensive methods capable of rapidly assessing all short-term instability mechanisms together. This necessity forms the foundation for the analysis presented in the following sections.

### *5.2. Evaluation Criteria for Short-Term Stability Indices*

A considerable number of approaches in the literature aim to address the problem of short-term instability. For any of these methods to be considered useful, they must demonstrate predictive capabilities that go beyond the straightforward information already available from raw voltage measurements. If no clear improvement is achieved, the method's cost–benefit ratio becomes unfavorable and unsuitable for practical adoption.

The considered approaches share a set of common characteristics. First, in order to ensure the fastest possible response, they rely exclusively on the direct processing of voltage measurements provided by PMUs; therefore, these methods typically avoid the estimation of power system parameters. For the same reason, they also aim to maintain numerical procedures as simple as possible, with the objective of minimizing computational burden. The absence of a network model, even in an estimated form, introduces a second feature: the indices inherently have a local nature. In other words, stability observability is restricted to the specific transmission lines where measurement devices are installed.

Next, several representative techniques for assessing short-term voltage stability are examined from a theoretical standpoint. The emphasis is placed on those methods most frequently cited in the literature and those with potential for real-time field application. Each method is compared against a set of qualitative criteria directly tied to effectiveness and practical deployment.

The first aspect is whether the technique requires knowledge of detailed system models. As modern grids are becoming increasingly complex and accurate models are rarely available in real-time, methods independent of system modeling are generally considered more advantageous.

Real-time feasibility is also a crucial requirement, as only methods capable of operating within tight timeframes can be realistically used for on-line monitoring. Another factor considered is the applicability of the methods to multiple forms of short-term instability, since adopting a unified evaluation framework is preferable. Equally important is the adaptability of these approaches to networks with high levels of renewable energy penetration, where the system dynamics are significantly altered, both in transmission and distribution domains.

Further comparison concerns the computational effort required. Ideally, methods should be kept computationally simple to minimize execution time, leaving sufficient

margin for corrective or preventive control actions. Excessive processing delays reduce the time available for mitigation.

To further enhance the time window available for the implementation of countermeasures, the sensitivity of the considered indices is also evaluated. Higher sensitivity enables the index to trigger earlier alarms within the control center, thus providing operators with a longer response horizon to initiate effective mitigation strategies.

Finally, the availability of validation results obtained from real-world data is considered an additional strength of an index. Indeed, an approach that demonstrates excellent performance under simulated conditions may not necessarily preserve the same characteristics when applied to measurements affected by realistic phenomena such as noise, uncertainty, or missing data.

### *5.3. Lyapunov Exponent*

The Lyapunov exponent (LE) originates from ergodic theory, a mathematical discipline concerned with deterministic dynamical systems and their statistical properties. It provides a tool to determine whether a system exhibits chaotic behavior at a given point in time by quantifying the rate at which nearby trajectories diverge. Owing to this property, the concept is broadly applicable to many classes of dynamical systems and has recently been suggested for applications in power system dynamics. Its basic formulation can be expressed as shown in Equation (63):

$$|\Delta V(t)| = e^{\lambda t}|\Delta V_0| \tag{63}$$

where $\lambda$ denotes the Lyapunov exponent, $\Delta V_0$ is the initial voltage perturbation, and $\Delta V(t)$ is the corresponding deviation in voltage trajectory at time $t$ [8].

In practice, only discrete voltage measurements are available; therefore, LE estimation is carried out using time-series data, commonly obtained from PMU recordings, according to Equation (64):

$$\lambda = \frac{1}{k\Delta t} \ln\left(\frac{|V'((n_0+k)\Delta t)|}{|V'(n_0\Delta t)|}\right) \tag{64}$$

Here, $k$ represents the window size expressed in number of samples, $\Delta t$ is the sampling interval, $n_0$ is the index of the first sample, and $V'$ is the voltage derivative at the given data point [8].

Equation (63) represents the theoretical exponential separation of two neighboring trajectories. In field measurements, however, two independently observed trajectories starting from infinitesimally close initial conditions are generally unavailable. The measurement-based formulation adopted in [8] therefore estimates a finite-time local growth rate over a moving observation window from the ratio of voltage-derivative magnitudes evaluated along a single measured trajectory. In this interpretation, the derivative acts as a local tangent-direction surrogate. Equation (64) should consequently be regarded as an operational finite-time estimator rather than as an exact reconstruction of the two-trajectory definition. Its reliability depends on local signal smoothness, adequate temporal resolution, dominance of the monitored dynamic component, and appropriate filtering, since numerical differentiation amplifies measurement noise.

A positive LE indicates instability at the monitored bus, whereas a negative value reflects stability. In power system studies, the largest (positive) Lyapunov exponent is often used, commonly referred to as the Maximum Lyapunov Exponent (MLE). A rigorous mathematical derivation of LE in the context of power grids can be found in [33,34].

There are two principal directions for applying LE in short-term instability monitoring. The first relies on monitoring bus voltages, as in Equations (63) and (64), which directly targets short-term voltage instability. The second employs the same mathematical frame-

work but substitutes voltages with rotor angles of synchronous machines, thereby enabling transient rotor angle stability assessment [35]. This dual applicability is advantageous, as emphasized in Section 2, since a unified methodology capable of covering multiple short-term instability mechanisms is highly desirable. Indeed, ref. [36] proposes a combined monitoring scheme for both voltage and rotor angle stability based on LE.

A key strength of the LE approach lies in its independence from detailed system models. Its reliance on measured quantities, primarily voltages, makes it robust to modeling errors and increasingly attractive given the rising complexity of modern grids. Additionally, the ongoing transition to renewable-based generation is unlikely to compromise its predictive performance, although the faster dynamics introduced by inverter-based resources may challenge the timeliness of accurate evaluations.

Nevertheless, one drawback is that computing derivatives inherently amplifies oscillations, leading to highly fluctuating LE values even when no true instability is present. This issue, observed in nearly all LE applications, complicates parameter selection and stability assessment.

The method has been assessed through simulation on the model of the provincial power grid at Guangdong in China.

Phase-Rectified Lyapunov Exponent

To mitigate the oscillations of the derivatives caused by noise and errors, ref. [37] proposes a phase-rectification method to smooth the LE without severely degrading its predictive capacity. The procedure leverages modal analysis techniques.

The voltage signal is modeled as a superposition of damped sinusoids:

$$v(n) = \sum_{i=1}^{p} A_i e^{\alpha_i n\Delta t} \cos(\omega_i n\Delta t + \varphi_i) \tag{65}$$

where $p$ is the model order, $A_i$ the amplitude, $\alpha_i$ the damping factor, and $\omega_i$ and $\varphi_i$ are the frequency and phase, respectively.

Parameters can be estimated using methods such as Prony's algorithm, the Matrix Pencil method, or the Hankel Total Least Squares (HTLS) approach. To enhance robustness, outputs from different engines are cross-validated, while a moving window of 1 s is used for analysis.

If a dominant mode exists, the derivative of the system trajectory can be expressed as:

$$v'(n\Delta t) = A_d e^{\alpha_d n\Delta t} \sqrt{\omega_d^2 + \alpha_d^2} \sin(\omega_d n\Delta t + \varphi_d + \theta_d) \tag{66}$$

With

$$\theta_d = \arctan\left(-\frac{\alpha_d}{\omega_d}\right)$$

Oscillations arise from the phase angle evolution. If the data window covers a full oscillation, derivatives at its endpoints share the same phase; otherwise, mismatches produce spurious variations.

To mitigate this, the derivative is normalized by the sinusoidal factor, yielding the envelope:

$$v'_{\max}(n\Delta t) = \frac{v'(n\Delta t)}{\sin(\omega_d n\Delta t + \varphi_d + \theta_d)} \tag{67}$$

The LE is then computed using the rectified derivative:

$$\lambda = \frac{1}{k \cdot N \cdot \Delta t} \sum_{i=1}^{N} \ln\left(\frac{v'_{\max}((i+k)\Delta t)}{v'_{\max}(i\Delta t)}\right) \tag{68}$$

where $N$ is a preset averaging factor. The overall algorithm consists of:

- Acquiring PMU voltage data and preprocessing with a moving average filter.
- Conducting modal analysis using multiple engines (Prony, Matrix Pencil, HTLS).
- Cross-validating outputs to ensure consistency.
- Verifying the existence of a dominant mode.
- Computing the derivative, and applying PR if a dominant mode exists.
- Estimating the LE using the PR-based or standard formula.
- Concluding stability if LE $< 0$, or instability otherwise.

While these refinements improve interpretability, they increase computational demands and shorten the already limited time window available for control actions.

Figure 9 demonstrates this effect, highlighting how the choice of data window size $k$ strongly impacts non-rectified LEs, potentially leading to ambiguous conclusions.

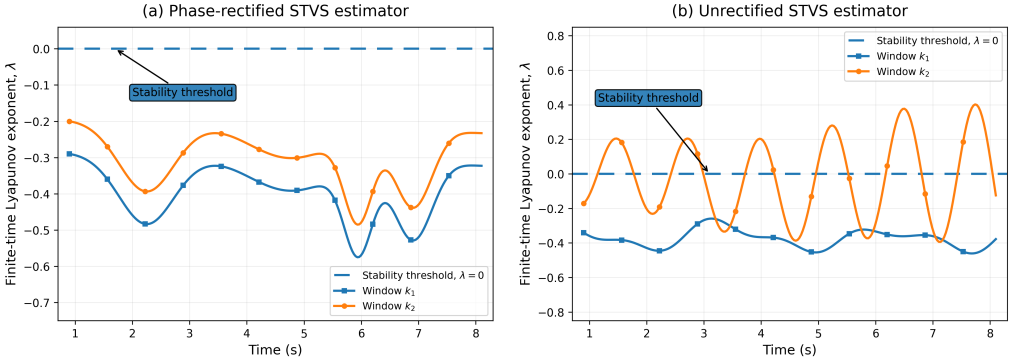



**Figure 9.** Illustrative comparison of finite-time Lyapunov-exponent estimates obtained with and without phase rectification for two moving-window settings, based on the phase-rectification method proposed in [37]. In the phase-rectified case, both estimates remain below the stability threshold, whereas the unrectified estimator may exhibit oscillations and spurious threshold crossings.

LE-based monitoring has also been tested in real-world conditions. For example, ref. [36] presents a practical framework for applying LE in live systems, addressing challenges such as parameter tuning and measurement noise. The cited study reports that the proposed LE-based implementation provided timely instability warnings; however, extending this success across diverse systems and operating states remains a significant challenge.

Ultimately, the central difficulty in using LE, as with other short-term stability metrics, is balancing accuracy with speed. Reliable detection requires precise data, yet shorter windows, while faster, reduce accuracy, and longer windows may delay countermeasures. Small inaccuracies in measurement or parameter estimation can produce disproportionately large errors, especially given the reliance on derivatives and the complexity of the computation.

### *5.4. Transient Voltage Deviation Index*

The second approach considered for short-term voltage stability assessment in this study is the Transient Voltage Deviation Index (TVDI). Originally introduced in [38], this quantitative metric evaluates both the magnitude of voltage deviations and the duration of the violation, offering a measure of the system's transient voltage behavior after a disturbance [39].

The formulation of the method is relatively simple and can be expressed through the following relations, given in Equations (69) and (70):

$$TVSI = \frac{\sum_{i=1}^{N} \sum_{t=T_c}^{T} TVDI_{(i,t)}}{N(T - T_c)} \tag{69}$$

where $N$ denotes the total number of buses in the power network, $T$ is the considered transient interval, $T_c$ indicates the instant of fault clearance, and $TVDI$ represents the transient voltage deviation index. The latter is defined as:

$$TVDI = \begin{cases} \dfrac{|V_{(i,t)} - V_{(i,0)}|}{V_{(i,0)}} & \text{if } \dfrac{|V_{(i,t)} - V_{(i,0)}|}{V_{(i,0)}} \geq \mu \\ 0 & \text{otherwise} \end{cases} \qquad \forall t \in [T_c, T] \tag{70}$$

Here, $V_{(i,t)}$ is the instantaneous voltage magnitude at bus $i$ at time $t$, $V_{(i,0)}$ is the corresponding pre-disturbance voltage, and $\mu$ is the threshold defining the boundary for unacceptable deviations. The study in [38] recommends a value of $\mu = 20\%$ although this parameter may vary depending on the specific system under consideration.

To better visualize the principle, Figure 10 provides a graphical representation of the method and highlights some of the parameters defined in Equations (69) and (70).

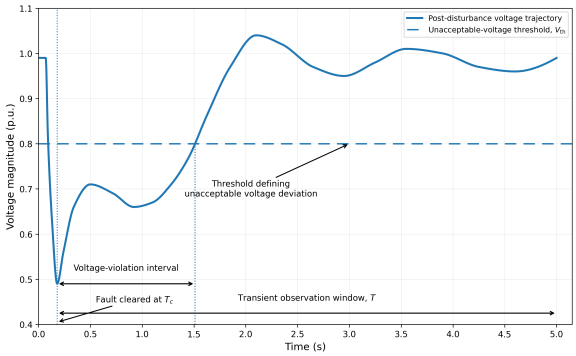



**Figure 10.** Illustrative post-disturbance voltage trajectory used to define the transient voltage deviation interval, based on the method presented in [38]. The voltage-violation interval extends from the fault-clearing instant $T_c$ to the first subsequent crossing of the unacceptable-voltage threshold $V_{\text{th}}$. The complete transient observation window is denoted by $T$.

In practice, the index shows a linear relationship with both the depth of the voltage dip and its duration. Consequently, larger deviations, whether in magnitude or in time, lead to higher index values, which reflect a deterioration in system stability. The metric has been widely adopted in the literature, with applications including dynamic VAR planning, demand response integration, and energy storage utilization [38]. It has also proven useful in more sophisticated frameworks, such as the dynamic security assessment within a Hierarchical Intelligent System described in [39].

The computation of the index requires reliable, accurate, and high-speed voltage measurements, making PMUs the most suitable data source. While it is inevitably affected by imperfections in the measurements, its sensitivity is considerably lower than that of derivative-based approaches. Another advantage lies in its model-free nature, which makes it, in principle, applicable to any type of power system.

Nonetheless, there are clear limitations. The most obvious is that the method only accounts for low-voltage conditions, being designed primarily for short-term voltage stability. As discussed in Section 2, however, short-term instabilities can take different forms that are often interrelated. For instance, in the case of oscillatory voltage profiles, TVDI may underestimate the severity of deviations, thereby reducing its value as an early-warning tool or as a control signal for predictive or corrective actions. This drawback could be partially addressed by extending the index to also incorporate overvoltage situations.

Furthermore, during Fault-Induced Delayed Voltage Recovery (FIDVR) events, the effectiveness of TVDI strongly depends on the threshold level adopted. Such events are not necessarily characterized by extremely low voltages; rather, they involve a prolonged

moderate undervoltage followed by a possible overvoltage spike, which in some cases precedes a voltage collapse. To properly capture the severity of these phenomena, a relatively high threshold is required. However, this may render the index overly sensitive to normal voltage fluctuations that do not pose real stability concerns.

TVDI represents a mathematically simple and computationally efficient measure for evaluating the severity of voltage dips. Despite its shortcomings, it provides richer insights than direct voltage monitoring alone and is likely to remain relevant for both present and future power systems, though further research is still needed.

The approach has been tested using the IEEE 39-bus New England system.

### *5.5. Trajectory Violation Integral*

The Trajectory Violation Integral (TVI) approach was originally introduced in [40]. Its mathematical formulation can be expressed as follows:

$$TVI = \int_{t_f}^{t_{end}} V_V(t)\, dt \tag{71}$$

where $t_f$ denotes the fault initiation time and $t_{end}$ is the duration of the dynamic simulation. The function $V_V(t)$ is defined in Equation (72):

$$V_V(t) = \begin{cases} T_{low}(t) - V(t) & \text{if } V(t) < T_{low}(t) \\ V(t) - T_{upp}(t) & \text{if } V(t) > T_{upp}(t) \\ 0 & \text{otherwise} \end{cases} \tag{72}$$

Here, $V(t)$ represents the actual voltage trajectory, while the bounding curves $T_{low}(t)$ and $T_{upp}(t)$ are exponential functions given by Equations (73) and (74):

$$T_{low}(t) = \frac{\left(\frac{t}{t_{end}} e^{\left(\frac{t}{t_{end}}\right)}\right)^{\beta}}{e^{\beta}} V_{st} \tag{73}$$

$$T_{upp}(t) = 2 - T_{low}(t) \tag{74}$$

where $\beta$ is a parameter controlling the exponential decay, and $V_{st}$ indicates the steady-state voltage level. At the system level, the overall index for $N_B$ buses is obtained as the summation of the individual TVI values, as shown below:

$$TVI_{tot} = \sum_{i \in N_b} TVI_i \tag{75}$$

A graphical illustration of the methodology is provided in Figure 11.

This approach introduces a novel idea by employing the integral of voltage deviations with respect to two exponential envelopes that represent the expected recovery path. In essence, it serves as a measure of how much the post-disturbance voltage trajectory diverges from these predefined exponential boundaries. As expected, it is necessary to know the disturbance onset time. In the literature, this is done by setting a trigger threshold on the voltage measures. Moreover, if, instead of a single disturbance, multiple overlapping disturbances occur, it becomes necessary to modify the shape or the amplitude of the voltage trajectory bounds.

The method captures both undervoltage and overvoltage conditions, while also accounting for the duration of the violation. Unlike fixed thresholds, such as those used in TVDI, the exponential bounds evolve with time: they are broader immediately after the disturbance and gradually tighten as the system approaches steady state. This feature makes

the index more practical, since large deviations occurring later in the recovery process are more indicative of instability, whereas early deviations are less critical.

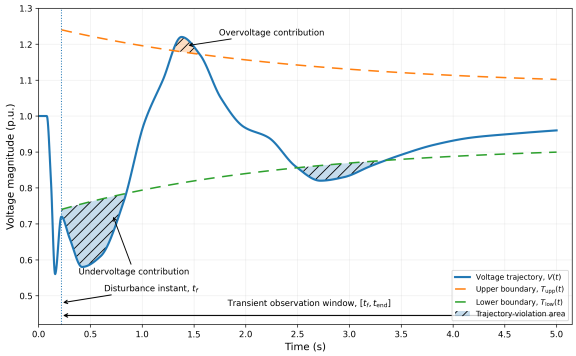



**Figure 11.** Illustrative representation of the Trajectory Violation Integral (TVI), based on the method presented in [40]. The time-varying boundaries $T_{\text{low}}(t)$ and $T_{\text{upp}}(t)$ define the admissible post-disturbance voltage recovery region. The shaded areas represent the contributions to the TVI when the voltage trajectory violates either the lower or the upper boundary.

As a result, the metric is likely well-suited to detect other forms of short-term instability described in Section 5. The use of exponential functions thus assigns greater weight to late post-fault variations, which is important for all four instability categories and cannot be achieved by static thresholds.

Another strength of the method is that it does not rely on system modeling, meaning it can in principle be applied to any bus where accurate and high-speed voltage measurements are available, independent of the share of inverter-based generation. However, while the index provides a clear quantification of short-term instability severity, the selection of appropriate parameters, particularly the instability threshold, is not trivial and strongly system dependent. As such, precise stability boundaries are difficult to establish. In addition, reliance on integral values makes the approach somewhat more complex and sensitive to measurement quality, speed, and possible errors.

The approach has been tested using the IEEE 39-bus New England system.

### *5.6. Contingency Severity Index*

The Contingency Severity Index (CSI), introduced in [41], is grounded in the WECC/NERC standards. Its purpose is to evaluate the severity of a voltage dip by jointly considering both its depth and its persistence. The method can be represented through the following equations:

$$CSI(t_f) = \frac{1}{n}\sum_{i=1}^{n}\left(w_{vi}SI_{vi}(t_f) + w_{ti}SI_{ti}(t_f)\right) \tag{76}$$

where $w_v$ and $w_t$ denote weighting coefficients, $n$ is the total number of buses, and the indices are defined as:

$$SI_v(t_f) = \begin{cases} \dfrac{|V_0 - V_{dev}|}{V_0} & \text{if } \dfrac{|V_0 - V_{dev}|}{V_0} \geq 0.3 \quad (0.25 \text{ if load bus}) \\ 0 & \text{otherwise} \end{cases} \tag{77}$$

$$SI_t(t_f) = \sum_{l_q \in L_{l_q}} \frac{\tau_{l_q}}{(t_f - t_{cl})} \tag{78}$$

Here, $V_0$ represents the pre-disturbance voltage level, $V_{dev}$ is the deviation caused by the fault, $t_f$ is the observation window, $t_{cl}$ is the clearing time of the disturbance, and $\tau_{l_q}$

represents the total duration of time intervals during which the voltage deviation remained below the safety threshold.

For a clearer explanation, Figure 12 illustrates two disturbance cases along with the corresponding calculation of $\tau$. In Case 2, $\tau$ represents the time interval during which the voltage remains below $0.8V_0$.

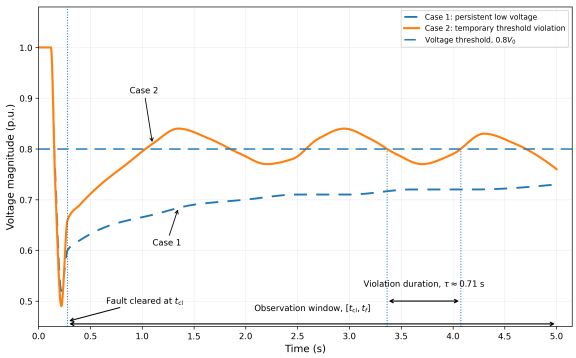



**Figure 12.** Illustrative voltage trajectories used to define the duration component of the Contingency Severity Index (CSI) based on the method presented in [41]. Case 1 represents a persistent post-disturbance low-voltage condition, whereas Case 2 exhibits temporary excursions below the threshold $0.8V_0$. The interval $\tau$ denotes the duration of one such threshold violation.

If, after the fault is cleared, the voltage never recovers above $0.8V_0$, the index reaches its maximum value of 1 (Case 1 in the figure). Further details can be found in [41].

When compared with the TVDI described in Section 5.4, the CSI is mathematically similar. The key distinction lies in the separate computation of the deviation magnitude and its duration, which are later aggregated in the final index. This separation makes it possible to apply different weighting factors. In [41], this property was exploited to determine the optimal placement of voltage support devices, using a mixed-integer dynamic optimization framework that incorporates CSI values as inputs.

### *5.7. Voltage Stability Risk Index*

The Voltage Stability Risk Index (VSRI) was first introduced in [42] as an indicator of long-term voltage stability and later applied in [43] for stability assessment and to determine optimal locations for load shedding.

The method is based on computing a moving average of bus voltages and then evaluating the normalized relative deviation of each sample with respect to this reference. The overall index value is obtained by accumulating the time-varying relative deviations.

Voltage instability typically appears first as a gradual reduction in voltage magnitude, which is eventually followed by a sharp drop at the point of system collapse. The phenomenon is strongly affected by overall system conditions as well as the behavior of individual components. Since voltage magnitude by itself does not provide a dependable indication of instability, relying solely on a fixed threshold to detect it can lead to misleading results. In this study, a dynamic stability criterion based on the VSRI [42] is employed to evaluate whether the system is capable of reaching a post-disturbance equilibrium state for bus voltages.

The VSRI is derived from the time-series data of the RMS values of load bus voltages within the system. Consider PMU measurements of a given load bus

$$y = [y_1, y_2, \ldots, y_N]^T$$

recorded at a phasor rate of 30 frames/s for a 60 Hz network and 25 frames/s for a 50 Hz network. The calculation of the VSRI proceeds through the following steps:

(a) Compute the moving average $v_j$ of the load bus voltage at the $j$th time instant, by taking the $N$ initial samples as a moving window across the total measured sample of $M$ on the available PMU data (with $N = 60$ adopted in this study).

$$v_j = \begin{cases} \dfrac{\sum_{k=1}^{j} y_k}{j} & j = 1, 2, \ldots, N \\ \dfrac{\sum_{k=j-N+1}^{j} y_k}{N} & j = N+1, \ldots, M \end{cases} \tag{79}$$

(b) Compute the percentage diversity $d_j$ between the voltage measured at $j$th instant and the moving average value

$$d_j = \frac{(y_j - v_j) \cdot 100}{v_j}, \qquad j = 1, 2, \ldots, M \tag{80}$$

(c) Calculate the $VSRI_j$ at $j$th instant by dividing the area under the percentage diversity curve by $N$ as follows:

$$VSRI_j = \begin{cases} \dfrac{\sum_{k=1}^{j} (d_k + d_{k-1})\Delta t/2}{j} & j \leq N \\ \dfrac{\sum_{k=j-N+1}^{j} (d_k + d_{k-1})\Delta t/2}{N} & N+1 \leq j \leq M \end{cases} \tag{81}$$

where $\Delta t$ is the subinterval in the above trapezoidal integral rule, and in this study, it is equal to 1.

When the index converges to zero, the system voltage is considered stable, while otherwise, it might be an indication of instability. Figure 13 and Figure 14 show an example of the index evolution with respect to the bus voltage variation under stable and unstable conditions, respectively.

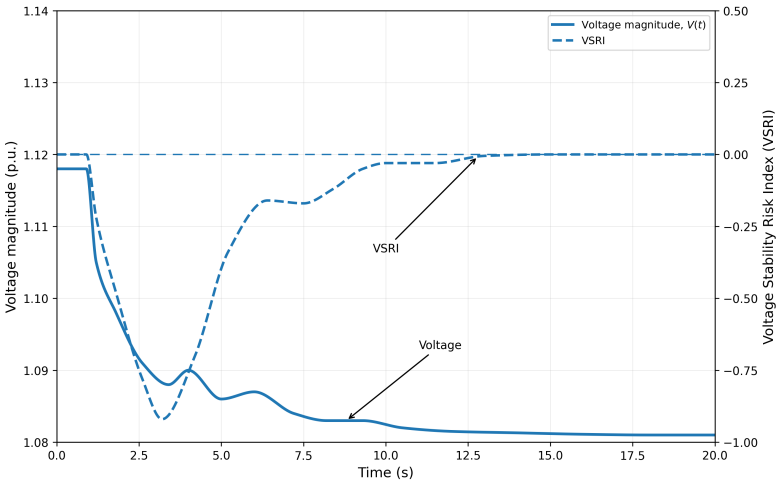



**Figure 13.** Illustrative evolution of bus-voltage magnitude and Voltage Stability Risk Index (VSRI) under stable post-disturbance conditions, based on the method presented in [43]. Following the transient voltage deviation, the VSRI progressively converges toward zero as the voltage trajectory approaches a quasi-steady-state condition.

Although the index was originally designed for long-term voltage stability assessment, the study in [43] demonstrated that it can also be applied to short-term voltage stability with reasonable accuracy and predictive capability in the scenarios examined. Nevertheless, the parameter configuration presented in that work is largely ad hoc, and its applicability to a broader range of systems and operating conditions remains uncertain.

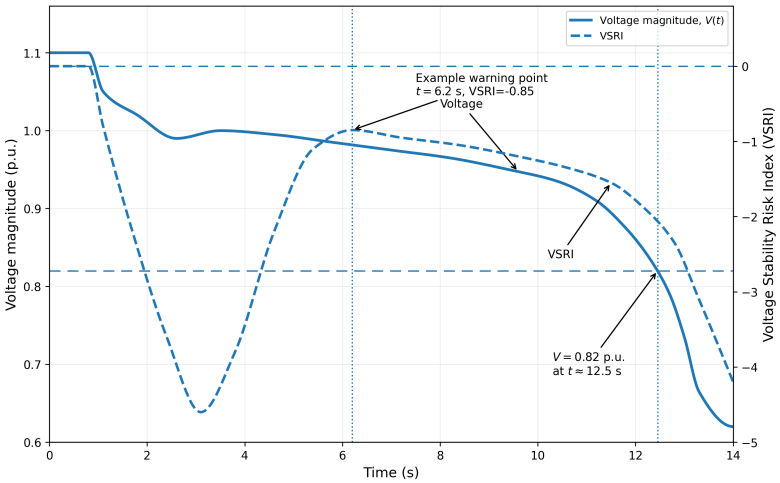



**Figure 14.** Illustrative evolution of bus-voltage magnitude and Voltage Stability Risk Index (VSRI) under unstable post-disturbance conditions, based on the method presented in [17]. Following an initial transient response, the VSRI does not converge toward zero and subsequently exhibits an increasing negative deviation, while the voltage magnitude progressively deteriorates toward a low-voltage condition. The indicated warning point and voltage threshold crossing are included for illustrative purposes.

From both a theoretical and practical standpoint, evaluating voltage deviations relative to a moving average can yield valuable insights into the state of the system. This approach is valid for both present-day and future grids, and it has the advantage of not requiring detailed knowledge of the underlying system structure.

However, whether the algorithm can consistently capture different types of short-term instabilities in modern power networks is still an open question. For example, oscillatory voltage behavior associated with transient rotor angle instability or converter-induced slow interaction instability may not be weighted as severely as warranted. A similar limitation may also arise in cases of fault-induced delayed voltage recovery (FIDVR).

The computational burden of the index itself is relatively low, but its effectiveness is strongly influenced by parameter selection—particularly the size of the moving average window and the threshold chosen to define instability.

The method has been tested on New England 39-bus system and a practical 246-bus Indian system.

### *5.8. AI- and Machine-Learning-Based Approaches*

In the last decade, the assessment of voltage stability in transmission networks has increasingly shifted towards data-driven approaches, motivated by the availability of high-resolution measurements from phasor measurement units (PMUs) and the growing computational capabilities offered by modern AI platforms. Unlike traditional analytical or model-based indices, which rely on detailed system models and extensive offline simulations, data-driven techniques attempt to learn the relationship between operating conditions and stability margins directly from historical or simulated measurement data. This paradigm has the advantage of bypassing some of the uncertainties associated with parameter estimation in large-scale networks, particularly in systems with high penetration of renewable energy, where accurate modeling is challenging. Early hybrid intelligent systems combining preprocessing and neural-network classifiers have also been proposed for power-system stability prediction [44]. More advanced methods such as deep neural networks (DNNs) [9] and convolutional neural networks (CNNs) [45] have been introduced to capture nonlinear dependencies and spatial correlations in voltage and current waveforms, while recurrent neural networks (RNNs) and long short-term memory (LSTM)

architectures [46] have been proposed for short-term voltage stability assessment processing the dynamic post-disturbance trajectories.

Recent research has also expanded towards ensemble methods, such as random forests and gradient boosting machines, which combine multiple weak learners to improve classification accuracy and robustness [47]. Another noteworthy direction is the application of graph neural networks (GNNs) [10], which are particularly suitable for power systems because they can explicitly incorporate the network topology into the learning process. By modeling buses as nodes and transmission lines as edges, GNNs can generalize across different grid topologies and operating conditions, offering a structured way to integrate domain knowledge with machine learning. Furthermore, unsupervised and semi-supervised learning methods have been explored to reduce the dependency on labeled data, for instance by clustering operating points or learning low-dimensional feature representations that correlate with voltage stability margins.

The advantages of these AI-based approaches are evident. Once trained, data-driven models can provide near real-time predictions of stability margins with minimal computational burden, which is crucial for wide-area monitoring and control applications. They are capable of handling large volumes of heterogeneous data, including synchronized PMU data, weather forecasts, renewable generation profiles, and load patterns, integrating information that would be difficult to combine in classical analytical indices. Additionally, data-driven methods offer flexibility and adaptability: models can be retrained or fine-tuned as new data becomes available, potentially keeping pace with evolving grid conditions. From a practical perspective, the ability of AI-based models to approximate nonlinear mappings means they have outperformed classical approaches in several reported test scenarios in terms of predictive accuracy, especially in scenarios involving highly stressed operating points or mixed generation portfolios.

However, despite these advantages, serious limitations prevent the widespread adoption of purely data-driven methods for operational use in voltage stability assessment. First and foremost, AI models rely on the availability of large, representative, and diverse datasets for training. Yet, real-world transmission systems rarely experience a sufficient number of voltage collapse or near-collapse events to create such datasets. While synthetic data generated by time-domain simulations can supplement real measurements, this approach risks embedding modeling assumptions and may not accurately reflect the dynamics of real power systems. Moreover, the non-stationarity of power grids represents a major challenge. The increasing integration of renewable energy sources and converter-based technologies significantly alters the inertia, damping, and dynamic response of transmission systems over time. As a result, an AI model trained on data representative of a given network configuration may quickly become obsolete as system conditions evolve, unless extensive retraining is performed. This problem is particularly acute in grids undergoing rapid transformations due to decarbonization policies and distributed generation.

Another critical issue concerns the interpretability and transparency of AI-driven indices. Operators and system planners often require methods that provide not only accurate predictions but also physical insights into the causes of instability. Traditional indices have the advantage of being rooted in system equations and therefore interpretable. In contrast, the "black-box" nature of many AI models makes it difficult to understand why a given operating point is classified as stable or unstable, which raises concerns in mission-critical applications. Furthermore, AI models are vulnerable to data quality problems, such as missing measurements, communication delays, or cyberattacks, which can compromise their reliability [48]. These aspects limit their acceptance among system operators, who prioritize robustness and trustworthiness over marginal gains in predictive accuracy.

From an operational perspective, the deployment of an AI-based voltage stability assessment tool cannot be reduced to a one-time training and inference process. An offline stage is required for scenario generation, data labeling, model training, and validation on operating conditions, network topologies, contingencies, and IBR penetration levels that were not included in the training set. The calibration of probabilistic or confidence outputs is also important, since an accurate classification without an indication of uncertainty may be insufficient for mission-critical decision making.

The online stage requires time alignment of PMU and SCADA data, bad-data detection, management of missing or delayed measurements, feature normalization, and monitoring for inputs that are outside the distribution represented in the training dataset. The model output should be accompanied by a confidence measure and, where possible, by physically interpretable information or by a comparison with conventional voltage stability indices. Periodic retraining, model versioning, cybersecurity assessment, and a validated fallback procedure are also necessary whenever the network topology, converter controls, or operating policies change. For these reasons, AI-based methods are more appropriately regarded at present as advisory or screening tools integrated with physics-based assessment, rather than as autonomous protection or control triggers [9,10,48].

For these reasons, although AI and ML techniques have shown considerable promise in academic studies and controlled simulations, their applicability to practical wide-area voltage stability monitoring remains limited. AI-based approaches have therefore been retained in the present review, but they are not identified as stand-alone candidates for immediate operational deployment. Priority is instead given to hybrid solutions that combine the data-processing capability of AI with physically interpretable indices, data-quality supervision, and operator-validated decision logic.

## 6. Comparative Summary of the Reviewed Methods

Several review papers have addressed specific aspects of voltage stability assessment, including classical static indices, PMU-based monitoring techniques, and data-driven approaches. In contrast, the present review aims to provide a unified perspective covering both long-term and short-term voltage stability assessment methodologies, with particular emphasis on converter-dominated transmission systems, the growing role of synchronized measurements, and the practical implementation issues associated with real-time operational environments. Furthermore, the paper discusses the complementary use of static and dynamic indicators, highlighting their respective applicability, computational requirements, and limitations under evolving grid conditions.

Tables 1 and 2 provide a comparative synthesis of the long-term and short-term voltage stability assessment methods discussed in the previous sections. The comparison highlights the information required for implementation, the main advantages and limitations, the degree of model dependence, and the suitability of each method for online monitoring. Its purpose is to support method selection by making explicit the trade-offs among physical interpretability, measurement requirements, computational burden, adaptability to changing operating conditions, and real-time feasibility.

### *6.1. Practical Workflow for Online Voltage Stability Monitoring*

An operational voltage stability monitoring process can be organized into five functional layers. The data-acquisition layer receives high-rate synchronized voltage and current phasors from PMUs together with slower SCADA measurements, equipment status signals, and network topology information. The preprocessing layer performs time alignment, timestamp and communication-latency checks, bad-data detection, filtering, missing-data handling, and disturbance-event detection.

**Table 1.** Summary of methods for long-term stability.

| Index | Information Required for Calculation | Advantages | Disadvantages |
|---|---|---|---|
| **L-index** | Nodal admittance matrix ($Y$); bus voltages (phasors); load currents/powers | Fast computation; good estimation of stability margin; possible to compute using PMU voltage and current data | Requires accurate $Y$; less precise in complex meshed networks |
| **Sensitivity Matrix** | Jacobian matrices ($\partial P/\partial\theta$, $\partial P/\partial V$, $\partial Q/\partial\theta$, $\partial Q/\partial V$); load-flow operating point | Identifies critical buses; works as early-warning indicator; applicable to the whole network | Requires accurate network model |
| **Modal Analysis** | Jacobian eigenvalues and eigenvectors | Identifies critical modes; provides global system insight | Computationally heavy (eigenvalue decomposition) |
| **Reactive Power Solvability** | Susceptance matrix; reactive powers at buses; voltage magnitudes | Strong physical interpretability; based on mathematical solvability conditions | Requires detailed network parameters; more complex to implement |
| **Minimum Distance to Instability** | Jacobian matrix and derivatives; iterative loading direction search | Quantifies the distance to voltage collapse; very accurate | Very high computational burden; not suitable for real time |
| **First and Second Derivative of Nodal Voltages** | Measured $V(t)$ time series; first and second derivatives | Model-free; very fast; good early-warning capability | Highly sensitive to noise; valid only for small disturbances |
| **Data-driven Model Estimation** | PMU voltage and current measurements; stochastic load statistics; time-series data | Does not require complete network model; adaptive to changing operating conditions; suitable for online monitoring | Requires high-quality PMU data; estimation accuracy depends on measurement quality and statistical assumptions |

**Table 2.** Summary of indices for short-term stability.

| Index | Information Required for Calculation | Advantages | Disadvantages |
|---|---|---|---|
| **Lyapunov Exponent (LE)** | Voltage time series; signal derivatives; moving analysis window | Model-free; can capture multiple instability mechanisms; also applicable to rotor-angle stability | Very sensitive to noise; strong oscillations in the derivative; hard to tune parameters |
| **Phase-Rectified Lyapunov Exponent (PR-LE)** | Modal decomposition (Prony, Matrix Pencil, HTLS); identification of dominant mode | Smoother and more robust than LE; improved interpretability | Higher computational burden; reduces the available reaction time |
| **Transient Voltage Deviation Index (TVDI)** | Voltage $V(t)$; pre-fault voltage $V_0$; safety threshold | Simple and robust; captures depth and duration of voltage dips | Cannot capture oscillatory behavior; strongly dependent on threshold choice |
| **Trajectory Violation Integral (TVI)** | Voltage $V(t)$; upper and lower exponential recovery bounds | Captures both undervoltage and overvoltage; adaptive thresholds reflect voltage recovery behavior; suitable for many types of instability | Requires tuning of parameters; higher computational effort |
| **Contingency Severity Index (CSI)** | Voltage $V(t)$; deviation magnitude; duration of violation; fault clearing time | Separates depth and duration; useful for optimizing VAR support placement | Depends on predefined thresholds; less generalizable across scenarios |
| **Voltage Stability Risk Index (VSRI)** | Moving average of bus voltage; relative deviation curve; area under deviation | Lightweight; model-free; good predictive capability in some systems | Strong dependency on window size; may not capture oscillations or slow deviations, e.g., FIDVR |
| **AI/Machine Learning Approaches** | Large historical or simulated datasets; PMU data streams; contextual data, such as load, RES, and weather | Very high accuracy; near real-time evaluation; learns nonlinear system behavior | Requires large, representative datasets; low interpretability; sensitive to missing data or cyber issues |

The assessment layer can include two parallel computational branches. A model-based branch updates the network representation and computes quasi-static indicators, such as the L-index or reduced-Jacobian and singular-value metrics, at the rate allowed by the state estimator and topology processor. A measurement-based branch processes high-rate PMU trajectories and calculates short-term indices after a disturbance has been detected. The two branches therefore operate on different time scales and should not be expected to provide numerically comparable outputs.

The outputs of the individual methods should not be interpreted directly as operational alarms. A decision layer should first associate each index with data-quality and estimation-confidence information and then apply operating-condition-dependent thresh-

olds, persistence criteria, and spatial-consistency checks. A fusion stage can combine the slower quasi-static stability margin with the faster post-disturbance trajectory information, identify the most critical buses or areas, and assign an alarm severity level. The resulting information can then be presented to the operator and linked to predefined remedial-action procedures while preserving operator supervision.

Measurements, calculated indices, alarm states, and operator actions should be finally archived. These records support periodic threshold recalibration, model validation, and the evaluation of false alarms and missed detections. The process described here represents a conceptual synthesis of the implementation requirements emerging from the reviewed literature and is not presented as a newly validated engineering framework [1,7,8].

### 6.2. Threshold Definition and Calibration

The difficulty of defining warning thresholds arises from both the intrinsic properties of voltage stability indices and the current limitations of calibration procedures. From an intrinsic perspective, most indices are proxy quantities whose relationship with an operational security boundary depends on network topology, loading direction, generation mix, converter-control modes, equipment limits, disturbance type, and assessment time scale. Even when a theoretical limiting value exists, such as the L-index approaching unity or the minimum singular value approaching zero, that value represents the mathematical collapse boundary rather than the earlier alarm level required for preventive operation.

For trajectory-based indices, the threshold, persistence time, moving window, or recovery envelope is often part of the index definition itself. These parameters determine the balance between sensitivity and false-alarm probability and therefore cannot generally be transferred unchanged between systems.

A second limitation concerns the available calibration methods. Warning levels are often derived from a finite set of offline simulations and may not adequately represent changes in topology, loading pattern, IBR penetration, control settings, or measurement quality. Context-dependent thresholds conditioned on the current operating state, together with probabilistic confidence intervals, persistence criteria, and spatial consistency checks, can improve adaptability. Nevertheless, such techniques reduce rather than eliminate system dependence. Threshold calibration should therefore be treated as a continuous operational process supported by representative simulations, archived events, and periodic performance assessment.

### 6.3. Joint Use of Singular-Value and Lyapunov-Based Indicators

The minimum singular value of the reduced Jacobian and an MLE-based indicator can provide complementary information, but their joint application requires two distinct computational paths. The singular-value branch depends on an updated network topology, state estimate, operating point, and Jacobian matrix. It is therefore suited to continuous quasi-static monitoring and can be used to identify progressive network stress and electrically weak areas.

The MLE branch instead processes high-rate synchronized voltage measurements following a detected disturbance. Its implementation requires signal filtering, numerical differentiation, an appropriate moving window, and sufficient PMU observability in the monitored area. It provides information on the local divergence or recovery of the measured trajectory rather than on the distance to a power-flow singularity.

Since the two outputs have different physical meanings, numerical scales, update rates, and uncertainty sources, they should not be combined by directly adding or averaging their numerical values. A decision-level fusion scheme is more appropriate. The quasi-static indicator can define the pre-disturbance stress condition and identify areas requiring closer

observation, while the dynamic indicator can provide event-triggered information on the subsequent voltage trajectory. Each output should be accompanied by data-quality and confidence information before a combined alarm level is assigned.

The principal implementation obstacles are the dependence of the singular-value index on topology and model accuracy, the sensitivity of MLE estimation to noise and parameter selection, incomplete PMU coverage, communication latency, time-alignment errors, and the need to validate joint alarm logic across representative contingencies. Consequently, collaborative implementation is technically feasible, especially where EMS and WAMS infrastructures are already integrated, but it is not a plug-and-play procedure and requires system-specific engineering and validation.

## 7. Conclusions

This review examined the principal methods and indices proposed for long-term and short-term voltage stability assessment in modern transmission systems, with particular attention to the increasing penetration of inverter-based resources and to the availability of synchronized measurements from PMUs and Wide Area Monitoring Systems. The reviewed approaches were compared in terms of their physical basis, information requirements, computational burden, applicability to real-time monitoring, and principal limitations.

For long-term voltage stability assessment, L-index, sensitivity, modal-analysis, singular-value, solvability, and distance-to-instability approaches provide physically interpretable information related to network loading and proximity to power-flow singularity. Their application in operational environments, however, depends on the availability and accuracy of the network model, reliable topology tracking, and the calibration of warning thresholds under different operating conditions. Data-driven estimation of network and Jacobian parameters may reduce the dependence on a fully specified model, but its applicability remains contingent on PMU coverage, measurement quality, system excitation, and the ability of the estimation procedure to follow changes in topology and operating point.

For short-term voltage stability assessment, Lyapunov-based and trajectory-based indices provide model-light or model-free means of processing post-disturbance voltage measurements. The studies reviewed in this paper report promising detection capabilities under the specific systems and disturbance scenarios considered. Nevertheless, their reported performance depends on the sampling rate, numerical differentiation and filtering procedures, moving-window length, disturbance type, and adopted decision thresholds. These dependencies should be carefully considered before transferring parameter settings or thresholds from one system to another.

Artificial-intelligence and machine-learning approaches can represent nonlinear relationships and support rapid stability classification. Their practical deployment, however, requires representative training datasets, adaptation to changes in network topology and operating conditions, sufficient interpretability, and resilience to missing, delayed, or corrupted measurements. These requirements currently limit the direct transfer of many results obtained in simulated environments to operational wide-area monitoring applications.

The reviewed literature does not identify a single voltage stability index that simultaneously satisfies all requirements related to physical interpretability, model independence, computational efficiency, adaptability, noise tolerance, and early-warning capability. The combined use of complementary quasi-static and dynamic indicators therefore represents a promising direction for wide-area monitoring, but it should not be interpreted as a universally validated solution. Its practical implementation requires time synchronization, data-quality assessment, consistent model and topology updates, operating-

condition-dependent thresholds, and validation against representative contingencies and field measurements.

Future research should therefore focus on reproducible benchmarking procedures, uncertainty quantification, adaptive threshold calibration, validation using realistic and field-derived datasets, and the integration of physically interpretable and data-driven methods into operator decision-support processes.

**Author Contributions:** Conceptualization, A.L., D.L., G.M.G. and G.C.; methodology, A.L., D.L., G.M.G., and S.T.; resources, A.L., D.L., and F.B.; writing—original draft preparation, A.L., D.L., and F.B.; writing—review and editing, all the authors; project administration, A.L., G.M.G., S.T., G.C., and C.P. All authors have read and agreed to the published version of the manuscript.

**Funding:** This research received no external funding.

**Data Availability Statement:** This study is a review of methods reported in the existing literature and does not involve the analysis of original experimental datasets. Synthetic data were generated solely for illustrative purposes in Figures 9–14 and are available from the corresponding author upon reasonable request.

**Acknowledgments:** During the preparation of this study, the authors used GenAI (ChatGPT 5.4 Version, OpenAI) for the purposes of generating Figures 1–3. The authors have reviewed and edited the output and take full responsibility for the content of this publication.

**Conflicts of Interest:** The authors declare no conflicts of interest. Author Guido Coletta, Giorgio Maria Giannuzzi, Salvatore Tessitore and Cosimo Pisani were employed by the company Terna. The remaining authors declare that the research was conducted in the absence of any commercial or financial relationships that could be construed as a potential conflict of interest.

## References

1. IEEE/CIGRE. *Evaluation of Voltage Stability Assessment Methodologies in Modern Power Systems with High Penetration of Inverter-Based Resources*; Technical Report Technical Brochure 943; CIGRE: Paris, France, 2024.
2. Hatziargyriou, N.; Milanović, J.; Rahmann, C.; Ajjarapu, V.; Cañizares, C.; Erlich, I.; Vournas, C. *Stability Definitions and Characterization of Dynamic Behavior in Systems with High Penetration of Power Electronic Interfaced Technologies*; Technical Report PES-TR77; IEEE PES: Piscataway, NJ, USA, 2020.
3. Boričić, A.; Torres, J.L.R.; Popov, M. Comprehensive Review of Short-Term Voltage Stability Evaluation Methods in Modern Power Systems. *Energies* **2021**, *14*, 4076. [CrossRef]
4. Ali, J.S.; Qiblawey, Y.; Alassi, A.; Massoud, A.M.; Muyeen, S.M.; Abu-Rub, H. Power System Stability with High Penetration of Renewable Energy Sources: Challenges, Assessment, and Mitigation Strategies. *IEEE Access* **2025**, *13*, 39912–39934. [CrossRef]
5. Kessel, P.; Glavitsch, H. Estimating the Voltage Stability of a Power System. *IEEE Trans. Power Deliv.* **1986**, *1*, 346–354. [CrossRef]
6. Van Cutsem, T.; Vournas, C. *Voltage Stability of Electric Power Systems*; Springer: Berlin/Heidelberg, Germany, 1998.
7. Vu, K.; Begovic, M.M.; Novosel, D.; Saha, M.M. Use of Local Measurements to Estimate Voltage-Stability Margin. *IEEE Trans. Power Syst.* **1999**, *14*, 1029–1035. [CrossRef]
8. Dasgupta, S.; Paramasivam, M.; Vaidya, U.; Ajjarapu, V. Real-Time Monitoring of Short-Term Voltage Stability Using PMU Data. *IEEE Trans. Power Syst.* **2013**, *28*, 3702–3711. [CrossRef]
9. Khodayar, M.; Liu, G.; Wang, J.; Khodayar, M.E. Deep Learning in Power Systems Research: A Review. *CSEE J. Power Energy Syst.* **2020**, *7*, 209–220. [CrossRef]
10. Hossain, R.R.; Huang, Q.; Huang, R. Graph Convolutional Network-Based Topology Embedded Deep Reinforcement Learning for Voltage Stability Control. *IEEE Trans. Power Syst.* **2021**, *36*, 4848–4851. [CrossRef]
11. Kundur, P. *Power System Stability and Control*; McGraw-Hill: New York, NY, USA, 1994.
12. Machowski, J.; Lubosny, Z.; Bialek, J.W.; Bumby, J.R. *Power System Dynamics: Stability and Control*, 3rd ed.; Wiley: Hoboken, NJ, USA, 2020.
13. Boričić, A.; Torres, J.L.R.; Popov, M. Fundamental Study on the Influence of Dynamic Load and Distributed Energy Resources on Power System Short-Term Voltage Stability. *Int. J. Electr. Power Energy Syst.* **2021**, *131*, 107141. [CrossRef]
14. Boričić, A.; Torres, J.L.R.; Popov, M. System Strength: Classification, Evaluation Methods, and Emerging Challenges in IBR-Dominated Grids. In *Proceedings of the 2022 IEEE PES Innovative Smart Grid Technologies Asia (ISGT Asia)*; IEEE: New York, NY, USA, 2022; pp. 185–189.

15. CIGRE WG B4.62. *Connection of Wind Farms to Weak AC Networks*; Technical Report Technical Brochure 671; CIGRE: Paris, France, 2016.
16. ENTSO-E. *Final Report on the Grid Incident in Spain and Portugal on 28 April 2025*; Technical Report; European Network of Transmission System Operators for Electricity (ENTSO-E): Brussels, Belgium, 2026.
17. Aslanian, M.; Hamedani-Golshan, M.E.; Haes Alhelou, H.; Siano, P. Analyzing Six Indices for Online Short-Term Voltage Stability Monitoring in Power Systems. *Appl. Sci.* **2020**, *10*, 4200. [CrossRef]
18. Hatziargyriou, N.; Milanović, J.; Rahmann, C.; Ajjarapu, V.; Cañizares, C.A.; Erlich, I.; Hill, D.J.; Hiskens, I.A.; Kamwa, I.; Pal, B.; et al. Definition and Classification of Power System Stability—Revisited & Extended. *IEEE Trans. Power Syst.* **2021**, *36*, 3271–3281. [CrossRef]
19. Gu, Y.; Green, T.C. Power System Stability with a High Penetration of Inverter-Based Resources. *Proc. IEEE* **2023**, *111*, 832–853. [CrossRef]
20. Li, Y.; Fu, L.; Meng, K.; Dong, Z.Y. Assessment and Enhancement of Static Voltage Stability with Inverter-Based Generators. *IEEE Trans. Power Syst.* **2021**, *36*, 2737–2740. [CrossRef]
21. Rokrok, E.; Qoria, T.; Bruyère, A.; François, B.; Guillaud, X. Transient Stability Assessment and Enhancement of Grid-Forming Converters Embedding Current Reference Saturation as Current Limiting Strategy. *IEEE Trans. Power Syst.* **2022**, *37*, 1519–1531. [CrossRef]
22. Huang, L.; Xin, H.; Dong, W.; Dörfler, F. Impacts of Grid Structure on PLL-Synchronization Stability of Converter-Integrated Power Systems. *IFAC-PapersOnLine* **2022**, *55*, 264–269. [CrossRef]
23. He, X.; Geng, H. PLL Synchronization Stability of Grid-Connected Multiconverter Systems. *IEEE Trans. Ind. Appl.* **2022**, *58*, 830–842. [CrossRef]
24. Dassios, I.K.; Cuffe, P.; Keane, A. Visualizing Voltage Relationships Using the Unity Row Summation and Real Valued Properties of the FLG Matrix. *Electr. Power Syst. Res.* **2016**, *140*, 611–618. [CrossRef]
25. Marconato, R. *Electric Power Systems*; CEI: Milano, Italy, 2008; Volume 3.
26. Simpson-Porco, J.W.; Dörfler, F.; Bullo, F. A Solvability Condition for Reactive Power Flow. In *Proceedings of the 2015 IEEE 54th Conference on Decision and Control (CDC)*; IEEE: New York, NY, USA, 2015; pp. 2013–2017.
27. Todescato, M.; Simpson-Porco, J.W.; Dörfler, F.; Carli, R.; Bullo, F. Optimal Voltage Support and Stress Minimization in Power Networks. In *Proceedings of the 2015 IEEE 54th Conference on Decision and Control (CDC)*; IEEE: New York, NY, USA, 2015; pp. 6921–6926.
28. Guo, J.; Pierrou, G.; Wang, X.; Du, M.; Wang, X. Data-Driven Methods in Modern Power System Stability and Security. In *Smart Cyber-Physical Power Systems*; Wiley: Hoboken, NJ, USA, 2025.
29. Pierrou, G.; Wang, X. An Online Network Model-Free Wide-Area Voltage Control Method Using PMUs. *IEEE Trans. Power Syst.* **2021**, *36*, 4672–4682. [CrossRef]
30. Yuan, Y.; Low, S.H.; Ardakanian, O.; Tomlin, C.J. Inverse Power Flow Problem. *IEEE Trans. Control Netw. Syst.* **2023**, *10*, 261–273. [CrossRef]
31. Boricic, A.; Torres, J.L.R.; Popov, M. Impact of Modelling Assumptions on the Voltage Stability Assessment of Active Distribution Grids. In *Proceedings of the 2020 IEEE PES Innovative Smart Grid Technologies Europe (ISGT-Europe)*; IEEE: New York, NY, USA, 2020; pp. 1040–1044.
32. Ravikumar, K.G.; Srivastava, A.K. Autonomous Detection of Fault-Induced Delayed Voltage Recovery Events. In *Proceedings of the 2024 IEEE Industry Applications Society Annual Meeting (IAS)*; IEEE: New York, NY, USA, 2024; pp. 1–6.
33. Wei, S.; Yang, M.; Qi, J.; Wang, J.; Ma, S.; Han, X. Model-Free MLE Estimation for Online Rotor Angle Stability Assessment with PMU Data. *IEEE Trans. Power Syst.* **2017**, *33*, 2463–2476. [CrossRef]
34. Khaitan, S.K. THRUST: A Lyapunov Exponents Based Robust Stability Analysis Method for Power Systems. In *Proceedings of the 2017 North American Power Symposium (NAPS)*; IEEE: New York, NY, USA, 2017; pp. 1–6.
35. Sayyeda, U.B.; Ghandhari, M.; Eriksson, R. Maximum Lyapunov Exponent Based Nearest Neighbor Algorithm for Real-Time Transient Stability Assessment. *Electr. Power Syst. Res.* **2024**, *234*, 110758. [CrossRef]
36. Safavizadeh, A.; Kordi, M.; Eghtedarnia, F.; Torkzadeh, R.; Marzooghi, H. Framework for Real-Time Short-Term Stability Assessment of Power Systems Using PMU Measurements. *IET Gener. Transm. Distrib.* **2019**, *13*, 3433–3442. [CrossRef]
37. Ge, H.; Guo, Q.; Sun, H.; Wang, B.; Zhang, B.; Liu, J.; Qian, F. An Improved Real-Time Short-Term Voltage Stability Monitoring Method Based on Phase Rectification. *IEEE Trans. Power Syst.* **2017**, *33*, 1068–1070. [CrossRef]
38. Xu, Y.; Dong, Z.Y.; Meng, K.; Yao, W.F.; Zhang, R.; Wong, K.P. Multi-Objective Dynamic VAR Planning Against Short-Term Voltage Instability Using a Decomposition-Based Evolutionary Algorithm. *IEEE Trans. Power Syst.* **2014**, *29*, 2813–2822. [CrossRef]
39. Xu, Y.; Zhang, R.; Zhao, J.; Dong, Z.Y.; Wang, D.; Yang, H.; Wong, K.P. Assessing Short-Term Voltage Stability of Electric Power Systems by a Hierarchical Intelligent System. *IEEE Trans. Neural Netw. Learn. Syst.* **2015**, *27*, 1686–1696. [CrossRef] [PubMed]
40. Verma, J.; Sharieff, I.; Sodhi, R. A meticulous approach towards contingency clustering in power system. In *Proceedings of the 2016 IEEE 7th Power India International Conference (PIICON)*; IEEE: New York, NY, USA, 2016; pp. 1–6. [CrossRef]

41. Tiwari, A.; Ajjarapu, V. Optimal Allocation of Dynamic VAR Support Using Mixed Integer Dynamic Optimization. *IEEE Trans. Power Syst.* **2011**, *26*, 305–314. [CrossRef]
42. Kim, D.J.; Moon, Y.H.; Kim, H.Y.; Yoon, Y. Voltage Stability Risk Index. U.S. Patent 7,236,898, 26 June 2007.
43. Seethalekshmi, K.; Singh, S.N.; Srivastava, S.C. A Synchrophasor Assisted Frequency and Voltage Stability Based Load Shedding Scheme for Self-Healing of Power System. *IEEE Trans. Smart Grid* **2011**, *2*, 221–230. [CrossRef]
44. Amjady, N.; Majedi, S.F. Transient Stability Prediction by a Hybrid Intelligent System. *IEEE Trans. Power Syst.* **2007**, *22*, 1275–1283. [CrossRef]
45. Tapia, E.A.; Colomé, D.G.; Rueda Torres, J.L. Recurrent Convolutional Neural Network-Based Assessment of Power System Transient Stability and Short-Term Voltage Stability. *Energies* **2022**, *15*, 9240. [CrossRef]
46. Zhang, M.; Li, J.; Li, Y.; Xu, R. Deep Learning for Short-Term Voltage Stability Assessment of Power Systems. *IEEE Access* **2021**, *9*, 29711–29718. [CrossRef]
47. Kunac, A.; Sarajcev, P. Ensemble Learning Approach to Power System Transient Stability Assessment. In *Proceedings of the 2020 5th International Conference on Smart and Sustainable Technologies (SpliTech)*; IEEE: New York, NY, USA, 2020; pp. 1–6.
48. Ren, C.; Du, X.; Xu, Y.; Song, Q.; Liu, Y.; Tan, R. Vulnerability Analysis, Robustness Verification, and Mitigation Strategy for Machine Learning-Based Power System Stability Assessment Model Under Adversarial Examples. *IEEE Trans. Smart Grid* **2021**, *13*, 1622–1632. [CrossRef]


**Disclaimer/Publisher's Note:** The statements, opinions and data contained in all publications are solely those of the individual author(s) and contributor(s) and not of MDPI and/or the editor(s). MDPI and/or the editor(s) disclaim responsibility for any injury to people or property resulting from any ideas, methods, instructions or products referred to in the content.